Thyroid hormones regulate the formation and environmental plasticity of white bars in clownfishes

Pauline Salis[a,b], Natacha Roux[a], Delai Huang[c,d], Anna Marcionetti[e], Pierick Mouginot[b,f], Mathieu Reynaud[g], Océane Salles[b,f], Nicolas Salamin[e], Benoit Pujol[b,f], David M. Parichy[c,d], Serge Planes[b,f], and Vincent Laudet[g,h,1]

[a]Observatoire Océanologique de Banyuls-sur-Mer, UMR CNRS 7232 Biologie Intégrative des Organismes Marins, Sorbonne Université Paris, 66650 Banyuls-sur-Mer, France; [b]Ecole Pratique des Hautes Etudes, Paris Siences et Lettres Research University, Université de Perpignan Via Domitia, CNRS, USR 3278 Centre de Recherches Insulaires et Observatoire de l'environnement, F-66360 Perpignan, France; [c]Department of Biology, University of Virginia, Charlottesville, VA 22903; [d]Department of Cell Biology, University of Virginia, Charlottesville, VA 22903; [e]Department of Computational Biology, University of Lausanne, 1015, Lausanne, Switzerland; [f]Laboratoire d'Excellence "CORAIL", F-66360 Perpignan, France; [g]Marine Eco-Evo-Devo Unit, Okinawa Institute of Science and Technology, Onna son, Okinawa 904-0495 Japan; and [h]Marine Research Station, Institute of Cellular and Organismic Biology (ICOB), Academia Sinica, I-Lan 262, Taïwan

Edited by Denis Duboule, University of Geneva, Geneva, Switzerland, and approved April 13, 2021 (received for review January 27, 2021)

Determining how plasticity of developmental traits responds to environmental conditions is a challenge that must combine evolutionary sciences, ecology, and developmental biology. During metamorphosis, fish alter their morphology and color pattern according to environmental cues. We observed that juvenile clownfish (*Amphiprion percula*) modulate the developmental timing of their adult white bar formation during metamorphosis depending on the sea anemone species in which they are recruited. We observed an earlier formation of white bars when clownfish developed with *Stichodactyla gigantea* (*Sg*) than with *Heteractis magnifica* (*Hm*). As these bars, composed of iridophores, form during metamorphosis, we hypothesized that timing of their development may be thyroid hormone (TH) dependent. We treated clownfish larvae with TH and found that white bars developed earlier than in control fish. We further observed higher TH levels, associated with rapid white bar formation, in juveniles recruited in *Sg* than in *Hm*, explaining the faster white bar formation. Transcriptomic analysis of *Sg* recruits revealed higher expression of *duox*, a dual oxidase implicated in TH production as compared to *Hm* recruits. Finally, we showed that *duox* is an essential regulator of iridophore pattern timing in zebrafish. Taken together, our results suggest that TH controls the timing of adult color pattern formation and that shifts in *duox* expression and TH levels are associated with ecological differences resulting in divergent ontogenetic trajectories in color pattern development.

pigmentation | developmental plasticity | clownfishes | thyroid hormones | metamorphosis

Understanding the origins of biodiversity is one of the major challenges of biology, but it should not be limited to the species level, which is however already a formidable task (1). Indeed, diversity is also present within species, as phenotypic variation between distinct populations and also within populations, depending on individual genotype and the extent to which physiology, behavior, or development are influenced by the environment (1, 2). In some instances, this phenotypic variation can reflect adaptive developmental plasticity that is defined as the ability of organisms to change their developmental trajectories to generate phenotypes precisely adjusted to the environmental conditions (1–3). Remarkable examples of such plasticity are known in animals, giving rise to distinct color patterns and other morphological traits, as well as life histories (4). For instance, different generations of butterfly can develop alternative color patterns on their wings depending on the season in which they emerge (5). Water fleas can grow large helmets and spikes as a response induced by predator cues, such as the concentration of kairomones in the water (6). Spadefoot toad tadpoles living in semiarid environments accelerate their metamorphosis in response to pond drying (7).

Determining how plastic developmental changes that occur in response to environmental conditions are coordinated at the physiological, cellular, and molecular levels is a challenge that must combine ecology with developmental biology (8, 9). The mechanisms that underlie the development of alternative phenotypes are still unclear for many systems and is one major goal of ecological developmental biology or ecological evolutionary developmental biology (1, 10).

Pigmentation is one of the conspicuous features of animals and often has clear ecological and behavioral significance. It is thus an outstanding model for understanding links between environment and developmental plasticity. There are several cases of teleost fishes exhibiting phenotypic plasticity in pigmentation (11). This is the case in cichlids, for which several species exhibit a conspicuous yellow-blue bright phenotype linked to social dominance (12), in the platyfish in which melanic spots phenotypes are polymorphic within and among populations of *Xiphophorus variatus* depending on stress status (13), in salmonids with various pigmentation phenotypes linked to stress and social dominance (14), and also in coral reef fishes such as the dottybacks depending on the presence of prey species (15).

One of the most extraordinary life history transitions in vertebrates is metamorphosis which is regulated by thyroid hormones

Significance

Developmental plasticity is defined as the ability of an organism to adjust its development depending on environmental signals, thus producing alternative phenotypes precisely adjusted to the environment. Yet, the mechanisms underlying developmental plasticity are not fully understood. We found that juvenile clownfish delay the development of their white bars during metamorphosis depending on the sea anemone species in which they are recruited. To understand this developmental plasticity, we investigated roles for thyroid hormones, the main hormones triggering metamorphosis in vertebrates. We found that thyroid hormones regulate white bar formation and that a shift in hormone levels, associated with ecological differences, results in divergent color patterns in different sea anemone species in which the young fish is recruited.

Author contributions: P.S., N.S., B.P., D.M.P., S.P., and V.L. designed research; P.S., N.R., D.H., M.R., O.S., and S.P. performed research; P.S., A.M., and P.M. analyzed data; and P.S. and V.L. wrote the paper.

The authors declare no competing interest.

This article is a PNAS Direct Submission.

[1]To whom correspondence may be addressed. Email: vincent.laudet@oist.jp.

This article contains supporting information online at https://www.pnas.org/lookup/suppl/doi:10.1073/pnas.2101634118/-/DCSupplemental.

Published May 24, 2021.

(TH) (16). With the very large number of TH-regulated morphological changes occurring during larval metamorphosis (17, 18), environmentally induced alterations to TH status during this developmental period have the potential to affect outcomes of the metamorphic process (19). TH is also required to shift the larval pigmentation toward adult pattern (20). In zebrafish, for instance, TH promotes the maturation of specific pigment cells, black melanophores, and yellow xanthophores (21). Whereas TH drives the terminal differentiation and proliferative arrest of melanophores, thus limiting their final number, it promotes the accumulation of orange carotenoid pigments in xanthophores, making the cells more visible (21, 22).

Here, we investigate the potential role of TH in a case of developmental plasticity in color morphs of clownfishes, and we tested the impact of two environments (e.g., sea anemone species) on that kinetic. Among these coral reef fishes, two closely related allopatric species, *Amphiprion ocellaris* and *Amphiprion percula*, live in mutualistic symbiosis with sea anemones in the tropical Indo-pacific (23, 24). We observed that *A. percula* young juveniles (referred to here as recruits) have a different rate of white bar formation depending on the sea anemone species, their obligate symbiotic partner, in which they are recruited: white bars develop more rapidly when fish are recruited in *Stichodactyla gigantea* than in *Heteractis magnifica*. Because *A. ocellaris* acquire their adult color pattern during metamorphosis (25, 26), we asked whether developmental plasticity in bar formation is associated with alteration in TH status. Using *A. ocellaris*, we found that blocking TH production delayed white bar formation, whereas excess TH accelerated white bar formation, revealing a role for TH in determining the rate at which color pattern shifts from larva to juvenile form. To test the ecological significance of these findings, we assayed TH titers and gene expression in wild-caught *A. percula* and found that young recruits associated with *S. gigantea* exhibited a higher level of TH and more abundant transcript of *duox*, a gene implicated in thyroid function and TH synthesis, as compared to recruits associated with *H. magnifica* (27). Further supporting a role for *duox* and TH in regulating the timing of iridophore patterning, we found that zebrafish deficient for *duox* activity were delayed in iridophore stripe formation relative to overall developmental progression. Taken together, our results suggest that TH regulates color pattern formation in clownfish and that shifts in hormone levels are associated with ecological differences that result in divergent ontogenetic trajectories in color pattern formation.

Results

Formation of White Bars of *A. percula* New Recruits Is Differentially Influenced by Age or Size Depending on Anemone Species. *Amphiprion* species acquire, in sequence, the head, body, and finally peduncle white bars during postembryonic development (26). In Kimbe bay, Papua New Guinea, *A. percula* is found in two different sea anemone hosts, *S. gigantea* and *H. magnifica*, and the fish living in these two hosts belong to the same population (28). We observed in the field that new *A. percula* recruits in *S. gigantea* have more white bars than new recruits in *H. magnifica* for juveniles of the same age and developmental stage (juvenile stage). In fact, 33% of 148 new recruits (200- to 250-d old) in *S. gigantea* had three white bars, whereas only 5% of 118 new recruits of the same age in *H. magnifica* had this pattern (Fig. 1 *A* and *B*, Test χ^2 $P = 0.0011$).

We tested by multiple regression whether sea anemone species affects the timing of white bar formation of *A. percula* new recruits from Kimbe bay while accounting for ecological and social structure variables. These results confirm our observations that new recruits had consistently more bars in *S. gigantea* than in *H. magnifica* for a similar age or size (Fig. 1 *C* and *D* and *SI Appendix*, Fig. S1 *A* and *B* and Tables S1–S4).

As illustrated in Fig. 1*C* and *SI Appendix*, Fig. S1*A*, the speed at which bands were acquired varies with age (or with size) and how the acceleration and deceleration of band acquisition varied with age (or size) also depends on the anemone species. Thus, our results indicate that anemone species differentially modulate the dynamic to which bars were acquired with age (or size). In fact, available data allow us to detect differences between anemone species in the shape of the relationship between bars and age (or size), but more data would be needed to fully characterize the shape of these relationships.

Adult Color Pattern Formation Is Linked to a Switch in Pigment Cell–Specific Gene Expression. Because we know that the sister species, *A. ocellaris* acquire their adult color pattern during metamorphosis (25, 26), we addressed whether TH is associated with developmental plasticity in color pattern using this species as a laboratory model (24, 25). *A. ocellaris* exhibits two pigmentation patterns during development: before stage 5 [around 9 days post hatching (dph) (25)], larvae have yellow larval xanthophores with a set of stellate larval melanophores forming two horizontal stripes covering the myotomes (Fig. 2 *A–D*, red arrowheads). From stage 5, larvae acquire, in a rostro-caudal temporal gradient, three white vertical bars (Fig. 2 *E–G*, white arrowheads), orange xanthophores outside of the future white bars (Fig. 2*E*, orange arrows), and melanophores dispersed all over the body (Fig. 2 *E* and *F*, black arrows) (25, 29). These melanophores are present over the body and are at higher density at the border of the white bars (Fig. 2 *F* and *G*).

To better understand color pattern changes occurring around stage 4, we assessed the expression of pigmentation genes across postembryonic stages. We extracted RNA from whole larvae at each of the seven *A. ocellaris* postembryonic stages and performed transcriptomic analysis (29). We focused on pigmentation genes defined by refs. 30 and 31 (Fig. 2*H* and *SI Appendix*, Fig. S2*A* and Table S5) and particularly on iridophore genes, as we showed previously that white bars are formed by iridophores (29) (Fig. 2 *I* and *J* and *SI Appendix*, Table S5). We observed that stages 1 to 3 are clearly separated from stages 4 to 7 along principal component 2 (Fig. 2 *H* and *I*, PC2). Among those genes, *fhl2b*, *pnp4a*, and *prkacaa* have a highest fold difference at stages 5 to 7 compared to stages 1 to 3, whereas *gbx2*, *trim33*, *gmps*, and *oca2* have a highest fold difference at stages 1 to 3 compared to stages 5 to 7 (Fig. 2*J*). We also observed a clear separation across stages for all the functional categories described in ref. 30 (*SI Appendix*, Fig. S2*A*): pigment cell specification (*SI Appendix*, Fig. S2*B*), xanthophore development (*SI Appendix*, Fig. S2*C*), and pteridine pigment synthesis of xanthophores (*SI Appendix*, Fig. S2*D*) as well as melanophore development (*SI Appendix*, Fig. S2*E*), melanogenesis regulation (*SI Appendix*, Fig. S2*F*), and, at a later stage, melanosome biogenesis (*SI Appendix*, Fig. S2*G*).These outcomes are consistent with changes across stages in pigmentation gene expression, complements of different pigment cell types, or likely both. They suggest that an important switch in the development of color pattern, involving each of the three pigment cells, occurs at stage 4.

White Bar Formation Is Controlled by TH Signaling. TH contributes to metamorphosis and the developmental program controlling pigmentation pattern in zebrafish and other teleosts (21, 32, 33). We hypothesized that TH regulates the timing of white bar formation during clownfish metamorphosis. To test this hypothesis, we exposed stage 3 larvae (5 dph) to different concentrations (10^{-6}, 10^{-7}, and 10^{-8} M) of the active TH, T3. After 3 d of treatment with T3, we observed a more-rapid appearance of white bars than in control larvae. This effect was dose dependent with, at 3 d posttreatment (dpt), 0% of the fish exhibiting two bands in the control, 50% at 10^{-8} M T3, 78% at 10^{-7} M, and 73% at 10^{-6}M (Fig. 3 *A–E*).

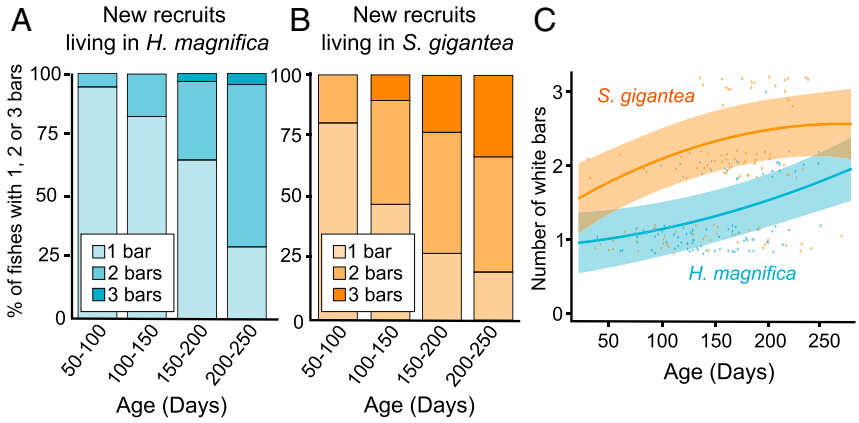

D

	H. magnifica		*S. gigantea*	
Parameter	Averaged β	85% C.I.	Averaged β	85% C.I.
Intercept	1.28	1.214; 1.345	1.511	1.393; 1.629
Age	0.067	-0.086; 0.35	0.481	0.108; 0.89
Age2	0.123	0.024; 0.351	-0.268	-0.774; -0.016
N_Fish	-0.037	-0.207; 0.026	-0.205	-0.307; -0.125
Female size	0.017	-0.02; 0.115	-0.015	-0.173; 0.069
Length difference	-0.003	-0.108; 0.084	0.023	-0.04; 0.177
Depth	-0.003	-0.077; 0.051	-0.006	-0.099; 0.056
Lagoon2	-0.002	-0.17; 0.124	0.667	0.478; 0.857
Lagoon3	-0.001	-0.168; 0.155	0.246	0.062; 0.43

Fig. 1. Formation of white bars of *A. percula* new recruits is differentially influenced by age depending on the anemone species. (*A* and *B*) Histograms representing percentage of new recruits having 1, 2, or 3 white bars depending on their age in new recruits living in *H. magnifica* (*A*) or *S. gigantea* (*B*). Statistical tests were done using χ^2 tests at each age between *H. magnifica* or *S. gigantea* and show statistical difference at 150 to 200 and 200 to 250 dph (respective $P = 0.0032$ and 0.0011). (*C*) Number of bars (85% CI) depending on age of individuals predicted from full averaging of the model candidates (*D*). Blue and orange represent respectively *A. percula* new recruits sampled in *H. magnifica* and in *S. gigantea*. The dots are observed data and are shifted around their number of bars for graphical representation. Predicted regressions of the number of bars are presented for the reference level "lagoon 0." (*D*) Full model averaged estimates (85% CI) of linear regression parameters from models including age for each anemone species. The parameter estimates after model averaging of treatment were compared with "Lagoon 1" as reference for the geographic zone. A parameter estimate whose 85% CI includes zero is considered uncertain, and parameter estimates whose 85% CI do not overlap are considered different.

We then tested the effect of decreasing TH signaling by blocking TH production with a mix of goitrogens (34). Larvae treated from stage 3 (5 dph) had a delay in white bar development compared to controls at 9 dpt (Fig. 3*H* compared to the control Fig. 3*G*): whereas 75% of controls had developed head and trunk white bars, only 15% of larvae treated with MPI (methimazol, perchlorate potassium and iopanoic acid) exhibited these bars, and the remainder were devoid of any bars (Fig. 3*F*). It should be noted that after 25 d of treatment, white bars ultimately formed in MPI-treated fishes, demonstrating that a delay rather than blockade in bar formation is associated with TH inhibition (Fig. 3*I*).

Pigment cells other than iridophores were also affected by TH treatment, with melanophore numbers increasing significantly within 48 h of treatment with 10^{-6} M T3 beginning at stage 3 (5 dph) (Fig. 3*J*; $P_{48hpt} = 0.0299$; $P_{72hpt} = 0.0043$). In contrast, MPI treatments led only to a minor decrease (nonsignificant) in melanophore numbers at 48 or 72 h posttreatment (hpt) (Fig. 3*J*). We did not observe gross differences in xanthophore development, and it was not possible to identify individual xanthophores or to quantify their numbers.

Taken together, these results suggest that TH controls the timing of white bar formation relative to overall somatic development and may act on iridophores and melanophores.

Expression of Pigmentation Genes Is Modified by T3 Treatment. To determine how TH affects iridophores, we assayed expression of iridophore genes [*fhl2a*, *fhl2b*, *apoda.1*, *saiyan*, and *gpnmb*; (29)] after treating larvae with exogenous TH. Stage 3 larvae were treated with T3 at different concentrations (10^{-6}, 10^{-7}, and 10^{-8} M) for 12, 24, 48 and 72 h, and expression of these genes was monitored by nanostring in RNA extracted from whole larvae. After T3 treatment, transcripts for all of these genes were significantly more abundant compared to levels in controls (*SI Appendix*, Fig. S3). In some cases (*apod1a* and *gpnmb*), this effect was evident by 12 h and in others (*fhl2a*, *fhl2b* and *saiyan*) only after 24 or 48 h. This suggests that TH affects expression of genes known to be expressed in clownfish iridophores.

Treatments with TH or Goitrogens Lead Respectively to Ectopic Iridophores over the Body and Decrease in White Hue in White Bars. To determine whether TH promotes iridophore differentiation, we treated stage 3 larvae with T3 at 10^{-6} M for a longer period to compare juveniles at stage 6, when fish have developed both head and body bars. Interestingly, head and body bars were never fully formed in T3-treated juveniles compared to controls (*SI Appendix*, Fig. S4*D* compared to *SI Appendix*, Fig. S4*A*), and close inspection of larvae revealed numerous ectopic iridophores across the flank of T3-treated fish (*SI Appendix*, Fig. S4*F* compared to *SI Appendix*, Fig. S4*C*, white arrowheads). Moreover, orange coloration was decreased in T3-treated juveniles compared to control (compare *SI Appendix*, Fig. S4 *B* and *E*). MPI treatment led to bars with normal shapes that were, nevertheless, more translucent presumably owing to deficiencies in the numbers of

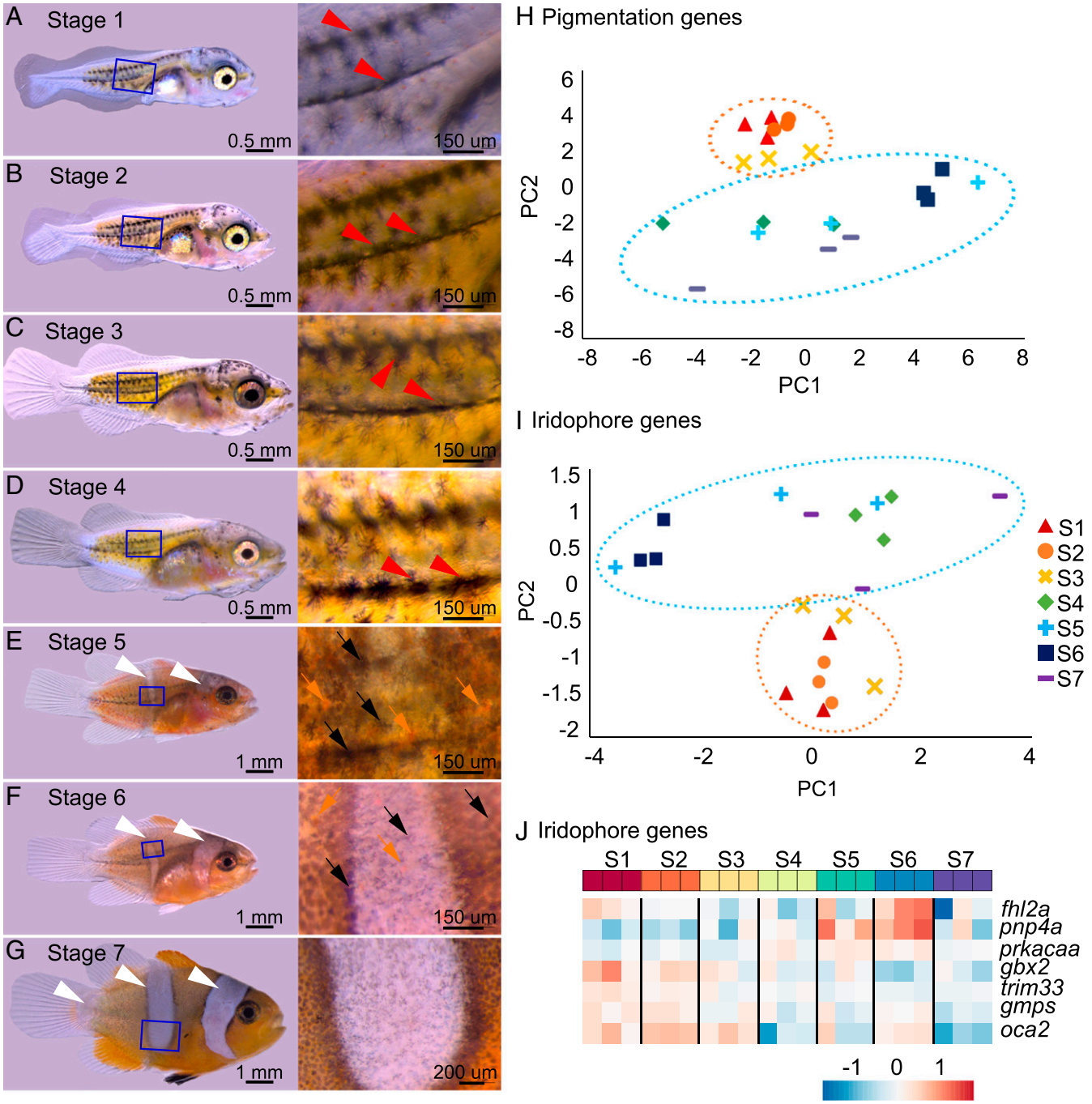

Fig. 2. Adult color pattern formation in *A. ocellaris* is linked to a switch in expression of pigment cells–specific genes during postembryonic development. (*A* and *B*) Stereomicroscope images of entire larvae and the associated zoom of the trunk at stage 1 (*A*), 2 (*B*), 3 (*C*), 4 (*D*), 5 (*E*), 6 (*F*), and 7 (*G*) (adapted from ref. 25). The white and red arrowheads point to white bars and black stripes and black and orange arrows point respectively to melanophores and xanthophores. (*H* and *I*) Principal component analysis (PCA) analysis of the pigmentation genes (*H*) and iridophores genes (*I*) expression from transcriptomic analysis from entire larvae over postembryonic stages. The two PCA exhibit a clear separation between stages 1 to 3 and stages 4 to 7. The ellipses were arbitrarily drawn around arrays to help resolution: stages 1 to 3 (orange) and 4 to 7 (blue) arrays. All stages had 3 replicates. (*J*) Heatmap of the seven iridophore genes having the highest fold change between stages 1 to 3 and stages 5 to 7. The color represents the intensity of the centered (but unscaled) signal that goes, for each gene, from low (blue) to medium (white) to high (red).

iridophores or the deposition of crystalline guanine within iridophores normally responsible for their white (or iridescent) appearance ($n = 2$, Fig. 3*I*).

Together, these results indicate that exogenous TH leads to reduced orange coloration and defects in white bar formation accompanied by ectopic iridophores on the body, whereas blockade of TH production leads to a reduced number of white iridophores or reflective guanine within white bars.

Ecological Modulation in Timing of White Bar Formation Is Linked to TH Levels and *duox* Expression. As TH treatment accelerated white bar development in *A. ocellaris*, we asked whether the accelerated acquisition of bars in *A. percula* recruits in *S. gigantea* was linked to TH. We sampled a second set of new recruits of 12 to 27 mm (having one white bar either complete or being formed) living either in *S. gigantea* ($n = 6$) or *H. magnifica* ($n = 6$) and measured TH levels. Concentrations of T3 (in picogram [pg]/g of

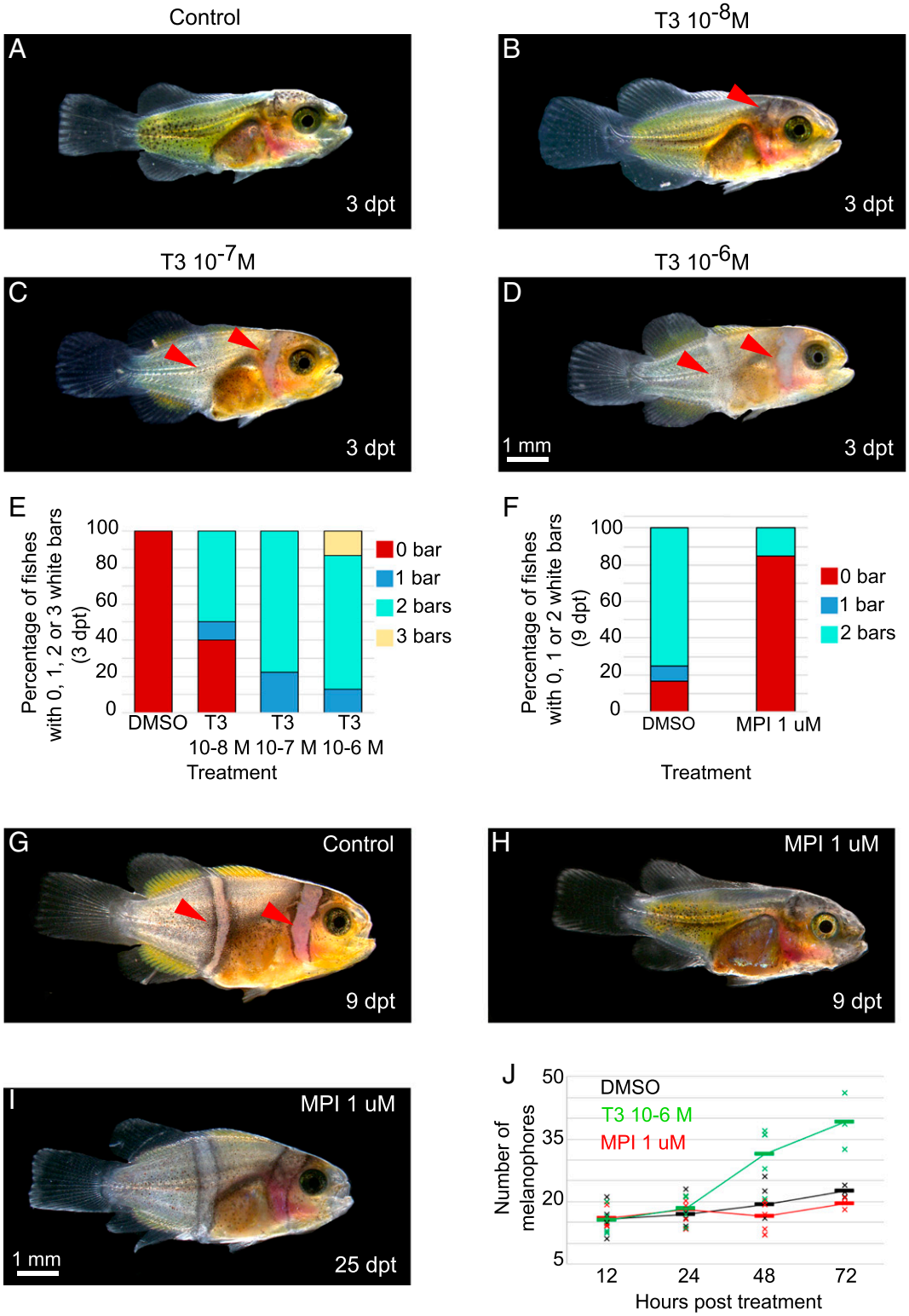

Fig. 3. White bars in *A. ocellaris* form earlier and later, respectively, after treatments with TH or goitrogens. (*A–D*) Stereomicroscope images of larvae treated at stage 3 during 3 d (dpt) in DMSO (*A*) or T3 at 10^{-6} (*B*), 10^{-7} (*C*), and 10^{-8} M (*D*). (*E* and *F*) Histogram showing the percentage of larvae having 0 (red), 1 (blue), 2 (turquoise), or 3 (yellow) white bars. (*E*) Larvae are treated at stage 3 for 3 d with DMSO, T3 10^{-6}, 10^{-7}, and 10^{-8} M (nDMSO = 16, nT3 10^{-8} M = 20, nT3 10^{-7} M = 18, nT3 10^{-6} M = 15 individuals). χ^2 tests are significant between T3 10^{-6} M and DMSO ($P < 0.0001$). (*F*) Larvae are treated at stage 3 for 9 d with DMSO or MPI 1 μM (nDMSO = 12, nMPI 1 μM= 13 individuals). Statistical test was done using χ^2 tests ($P < 0.0029$). (*G–I*) Stereomicroscope images of larvae treated at stage 3 during 9 d in DMSO (*G*) and MPI 1 μM (*H*) and MPI 1 μM stage 3 larvae treated for 25 d (*I*). (*J*) Graphic showing the number of melanophores in a specific area of the trunk in DMSO (black), T3 10^{-6} M (green), and MPI 1 μM (red) at 12, 24, 48, and 72 hpt (nDMSO > 9, nT3 > 9, nMPI > 9 individuals). The statistical tests were done using ANOVA between the T3 or MPI treatments and DMSO (control) at each time. The tests are significant between T3 and DMSO at 48 hpt and 72 hpt (*P* are respectively equal to 0.0299 and 0.0043). The bars correspond to the mean, and crosses correspond to one experiment. hpt = hours posttreatment (scale bar, 1 mm).

larvae) were significantly greater in new recruits sampled from *S. gigantea* compared to the those from *H. magnifica* (Fig. 4*A*).

To gain insight into mechanisms that explain these differences, we compared gene expression between *A. percula* new recruits found in *H. magnifica* ($n = 3$) or *S. gigantea* ($n = 3$) by RNA sequencing (RNA-Seq) of whole fish. Out of the 19,063 analyzed genes, only 21 were significantly more expressed in new recruits from *S. gigantea* (adjusted $P < 0.05$, $Log_2FC > 1$), while 15 were significantly more expressed in new recruits from *H. magnifica* (adjusted $P < 0.05$, $Log_2FC < 1$) (Fig. 4*B* and *SI Appendix*, Table S6). Within the differentially expressed genes, we observed *duox*, which encodes a dual oxidase implicated in TH production (27, 35). This gene was significantly overexpressed in new recruits from *S. gigantea* (adjusted $P = 0.038$, $Log_2FC = 2.53$) compared to those from *H. magnifica*. Together, these results suggest that the rate of white bar formation in *A. percula* is linked to a differential level of T3, which is in turn linked to a differential expression of *duox*.

Last, we wanted to directly test whether *duox* is required for iridophore patterning. For this, we used zebrafish *Danio rerio*, in which iridophores depend on TH for their maturation (22). *duox* requirements have been described for somatic development and melanophore numbers but not iridophore pattern (27, 35). We therefore injected one-cell stage embryos of the iridophore reporter line Tg(*pnp4a:palm-mcherry*)^{wpr110Tg} with highly efficient Alt-R CRISPR-Cas9 (36) targeting *duox*, resulting in phenotypes concordant with those for this locus (27, 35) and other hypothyroid fish (21, 22). Fig. 4*C* shows mCherry+ iridophores (dark cells; pixel values inverted) in representative uninjected (wild type) and *duox*-deficient larvae of the same stage [10.6-mm standard length (SL)]. In wild type, densely packed iridophores have formed one complete interstripe and a second interstripe has

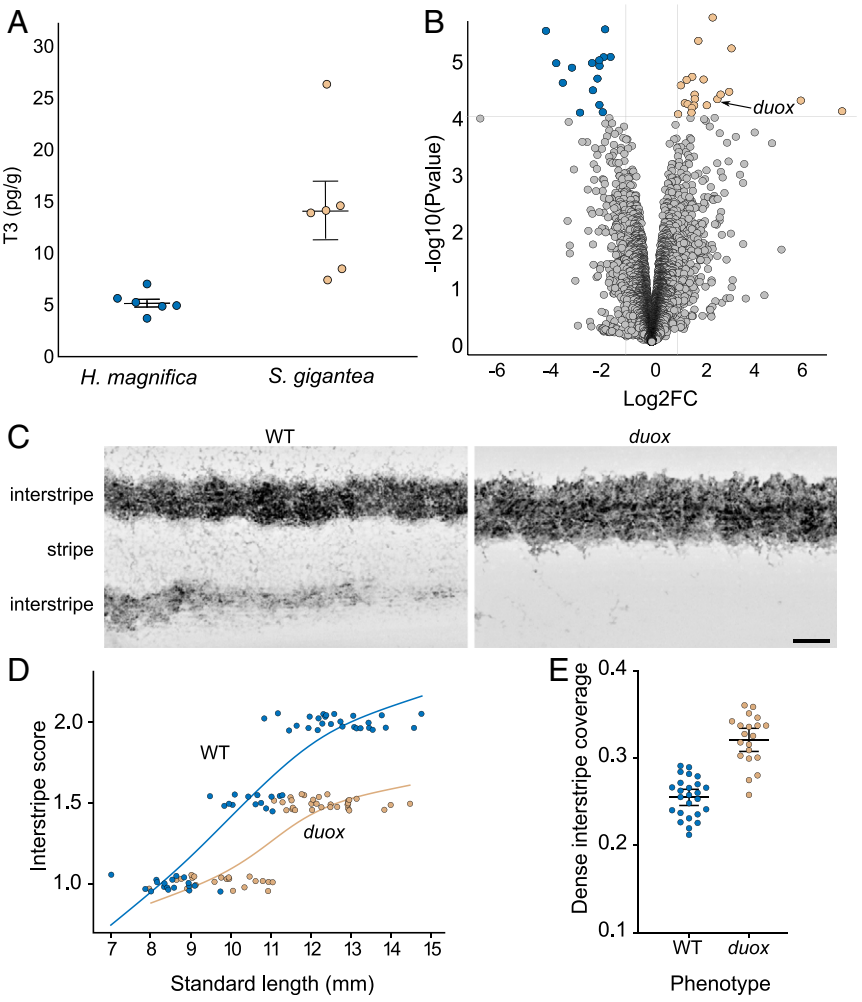

Fig. 4. *duox* requirement for the timing of color pattern formation in zebrafish. (*A*) Graph representing T3 level (in pg of T3 normalized by the weight of the fish in g) in *A. percula* new recruits sampled in *H. magnifica* or *S. gigantea* (nonparametric Mann–Whitney *U* test, $P = 0.0022$). (*B*) Volcano plot of differentially expressed genes between *A. percula* new recruits living in *H. magnifica* or *S. gigantea*. Positive Log2FC values correspond to an increased expression in recruits from *S. gigantea*, while negative Log2FC corresponds to increased expression in recruits from *H. magnifica*. The blue and yellow points correspond to significantly differentially expressed genes. The vertical black lines delimit the Log2FC threshold of 1, while the horizontal line corresponds to the corrected *P* threshold. (*C*) Inverted fluorescence images show iridophores (dark cells) marked by *pnp4a:mem-mCherry* expression at 10.6-mm SL in wild-type (*Left*) and *duox* CRISPR/Cas9 mutants of zebrafish *D. rerio* (*Right*). (*D*) Numbers of interstripes were scored qualitatively over SL in wild-type (blue, $n = 61$) and *duox* CRISPR/Cas9 zebrafish mutants (yellow, $n = 51$). Complete interstripes received a score of 1 and developing interstripes received a score of 0.5. Each circle represents a single individual and points are jittered vertically for clarity, and equivalently smoothed splines are shown for ease of visualization. The differences in total numbers of interstripes and tractories of interstripe addition resulted in significant effects of genotype (likelihood ratio test, $\chi^2 = 91.7$, $P < 0.0001$, degrees of freedom [d.f.] = 1) and genotype × SL interaction ($\chi^2 = 21.9$, $P < 0.0001$, d.f. = 1). (*E*) Despite having fewer interstripes overall, *duox*-deficient zebrafish had proportionally more of the flank covered by dense, interstripe iridophores as compared to the wild type ($F_{1,43} = 76.1$, $P < 0.0001$). The bars indicate means ± 95% CIs (scale bar in *A*, 200 μm).

started to form ventrally; some loosely arranged iridophores occur in between, where a melanophore stripe develops (37). In the *duox*-deficient larva, only a single wider interstripe has developed and fewer stripe iridophores are visible (Fig. 4*C*), suggesting that iridophore development is slowed in *duox*-deficient animals. Consistent with this interpretation, most wild-type fish greater than 11.0-mm SL had developed two complete interstripes (score = 2.0), whereas equivalently staged *duox*-deficient fish had developed only one complete interstripe and were still developing a second interstripe (score = 1.5) (Fig. 4*D*). Despite having fewer interstripes overall, *duox*-deficient animals had proportionally more of the flank covered by dense, interstripe iridophores, as compared to the wild type (Fig. 4*E*). These data show that *duox*, presumably acting through TH (27, 35), contributes to the timing of iridophore interstripe appearance and the patterning of interstripes in zebrafish.

To conclude, our findings suggest that reduced abundance of *duox* transcript in *A. percula* recruits within *H. magnifica* in comparison with those that are recruited in *S. gigantea* leads to a delay in the development of their white bars. This effect of *duox* in regulating the timing of iridophore development is conserved between the distantly related clownfish and zebrafish.

Discussion

During postembryonic development, *A. ocellaris* lose their larval color pattern and acquire in a few days and in a rostro-caudal sequence the head, body, and caudal peduncle white bars of their final adult color pattern. We showed here that during clownfish metamorphosis, the formation of iridophore-containing white bars that are formed by iridophores is accelerated by TH and that THs also underlie environmental (e.g., sea anemone species) plasticity in bar formation in wild populations. Interestingly a corresponding effect on iridophore patterning was also seen in zebrafish: *duox* mutants are hypothyroid (27, 35), and we found that iridophore patterning of *duox*-deficient animals was delayed. All these data converge toward the notion that variations in TH levels control a plastic pigmentation phenotype observed in clownfishes.

The observation that in both clownfish and zebrafish, TH affects white bar (clownfish) or interstripe (zebrafish) formation strongly suggests that these hormones directly or indirectly act on iridophores. Previous studies revealed that TH deficiency in zebrafish leads to an excess of melanophores and a loss of visible xanthophores (21). Further analyses showed that these hormones act differently on these two cell types, promoting maturation but via distinct mechanisms. TH promotes terminal differentiation and limits the final number of melanophores, whereas it promotes accumulation of carotenoid pigments in xanthophores, making initially unpigmented precursors visible. A similar role for TH in promoting iridophore maturation was suggested by analyses of single-cell transcriptomic states, though consequences for iridophore number and pattern were not assessed (22). In our analysis we observed that interstripe development is slowed in *duox*-deficient animals and that *duox*-deficient animals had proportionally more of the flank covered by dense, interstripe iridophores as compared to the wild type. Together, these several observations support the idea that TH signaling has an evolutionarily conserved role in regulating the timing of iridophore development in two species having markedly different adult pigment patterns. TH receptors are expressed in iridophores of both species, but analyses to date cannot indicate whether effects of TH are direct or mediated through other cell types (22).

We also observed an effect of TH on the shape of the trunk white bars in clownfish. Indeed, late in TH-treated fishes, we observed abnormalities in this trunk white bar that is misshapen and incomplete (e.g., it does not cross the full body of the fish; *SI Appendix*, Fig. S4*D*). This is interesting as a similar phenotype is often observed in clownfish juveniles raised in the laboratory and has been assumed to result from nutritional defects (38–40). In addition to abnormalities in the shape of white bars, we observed ectopic iridophores. We cannot exclude at this point that the defects in white bar shape could be linked to a role of TH on pigment cells migration.

We have observed that *A. percula* developing in association with *S. gigantea* acquire faster their white bars and have higher levels of T3 than *A. percula* in *H. magnifica*. This difference can be explained by higher expression of *duox* by *A. percula* recruited in *S. gigantea* as compared to *A. percula* recruited in *H. magnifica*. Indeed, *duox* encodes a dual oxidase that has been implicated in TH production both in mammals and zebrafish (27, 35). Beyond the effects of *duox* inactivation we observed on zebrafish iridophore patterning, *duox* mutants have growth retardation, ragged fins, thyroid hyperplasia, and infertility and a pigmentation phenotype with increased melanophore and reduced xanthophore (27, 35) typical of hypothyroid fish (21). As shown by Chopra et al., some of these defects can be rescued with T4 treatment, even when initiated in adult fish (27). All these data allow us to suggest that in young juveniles which are recruited in *S. gigantea*, there is an increased expression of *duox* that led to a higher TH level and a higher rate of white bar formation.

The results of our study leave two major questions unanswered: why is there an increased *duox* expression in *S. gigantea* recruits, and is there ecological significance to faster white bar formation in those fish? The regulation of *duox* gene expression in fish is still poorly known, but it has been shown that *duox1* and *duox2* expression in mammals is tightly controlled and regulated by thyroid-stimulating hormone, that is the hypothalamo–pituitary–thyroid axis (41). As *S. gigantea* has been shown to be a much more toxic sea anemone than *H. magnifica* by hemolytic and neurotoxicity assays (42), it is conceivable that clownfish recruited in this sea anemone perceive this harsher environment and hence activate their neuroendocrine axis to compensate. It is important to note in that respect that several anemonefish adults (*A. percula* but also *Amphiprion clarki*, *Amphiprion polymnus*, or *Amphiprion chrysopterus*) exhibit a similar polymorphic melanistic morph when present in *Stichodactyla* versus *Heteractis* (43). It is tempting to propose that these melanistic morphs are also linked to TH signaling in these species. The white bar phenotype we discussed here is therefore likely to be only one of a series of changes linked to the differential recruitment in various sea anemone species that allow the physiological adjustment of the fish in these distinct environments (44). However, the adaptative significance of this plastic phenotype is still only a hypothesis that remains to be tested experimentally in the field (44). It is interesting to note that *A. ocellaris* can also live in the same two sea anemone species but does not exhibit a melanistic morph when present in *Stichodactyla* (45). The rate of white bar appearance in young recruits of *A. ocellaris* living in the two sea anemone species is unknown. It will be interesting to study in the future the differences in pigmentation plasticity between the two sister species, *A. ocellaris* and *A. percula*.

In conclusion, our study of white bar formation in clownfish highlights the interest of this emerging system to investigate the cellular, molecular endocrine, and developmental basis of alternative phenotypes that are detected in natural situation (24, 46). Combining analysis in the wild as well as in the laboratory, as we have done here using clownfish as model, offers great promises to understand the evolutionary and developmental basis of plastic phenotypes often observed in nature.

Materials and Methods

See extended methods provided in *SI Appendix*.

***A. ocellaris* Larval Rearing and Ethics.** *A. ocellaris* were maintained as described in ref. 25. We have approval for these experiments from the C2EA-36 Ethics Committee for Animal Experiment Languedoc-Roussillon (CEEA-LR), number A6601601. The experimental protocols were following French regulation.

RNA Extraction and Transcriptomic Analysis. Transcriptomic data of developmental stages of *A. ocellaris* larvae were taken from the transcriptomic analysis of *A. ocellaris* postembryonic stages performed in ref. 29. For more information, see *SI Appendix*. Individuals of *A. percula* new recruits were sampled, euthanized in a MS222 solution (200 mg/l), and conserved in RNAlater. Total RNA of each individual was extracted using (TRIzol Reagent 15596-026 kit, Ambion) followed by DNase treatment (DNA-free AM1906 kit, Ambion) and then purified with 0.025-μm dialysis membranes. RNA-Seq libraries and sequencing were performed on an Illumina HiSeq 4000 sequencer using a stranded protocol as paired-end 50 base reads. Transcriptomic analysis is described in *SI Appendix*.

Drug Treatment of *A. ocellaris* Larvae. T3 (3,3′,5-Triiodo-L-thyronine) and IOP (Iopanoic Acid) were both diluted in dimethyl sulfoxide (DMSO) (T3: T2877, IOP: 14131, DMSO: D8418; Sigma-Aldrich) to a final concentration of 1 mM. To analyze the effect of a reduction of TH signaling, we used a mix of goitrogens called MPI as in ref. 47. Methimazole, potassium perchlorate, and IOP (Methimazole: M8506 and Potassium perchlorate: 460494; Sigma-Aldrich) were also diluted in DMSO to a respective final concentration of 100, 10, and 1 mM. Larvae were treated from 5 until 18 dph in 0.005% DMSO with T3 + IOP at 10^{-6}, 10^{-7}, and 10^{-8} M (respective dilutions of 1/1,000, 1/10,000, or 1/100,000) or MPI (dilution of 1/1,000) or without (controls). For each condition, five larvae were treated in 500-mL fish medium in a beaker. Each day, 100 mL of solution were changed.

Nanostring Gene Expression Analysis. A total of 400 ng total RNA were analyzed using the Nanostring Counter. Each sample was analyzed in a separate multiplexed reaction including eight negative probes and six serial concentrations of positive control probes. Data were imported into nSolver software (version 2.5) for quality checking and data normalization according to NanoString guidelines. Analysis was done using the R package TTCA1 (R version 3.5.1).

Effect of Ecological Factors on the Number of Bars in New Recruits of *A. percula*. At the time of the sampling in Kimbe bay (5°12′22.56″ S, 150°22′35.58″ E), West New Britain Province, Papua New Guinea, we characterized the new recruit size, age (*SI Appendix*), ecological variables (geographic zone, primary host anemone species, and depth), and the social structure of the new recruits within its sea anemone (total number of conspecifics inhabiting the sea anemone, size difference between the new recruit and the last subadult in the social hierarchy, female size) (28, 48). In the studied *A. percula* colonies located in Kimbe, 43% are in *S. gigantea* and 57% in *H. magnifica*. To assess what factors affect the number of bars on new recruits, we modeled the number of bars as a response variable depending upon either size or age, their squared value, and ecological and social structure independent variables. We followed a multimodel inference approach (49, 50) to estimate predictors effect sizes and their 85% CI (51). This approach was conducted independently in each anemone species to avoid confounding effects between anemone species and depth (see *SI Appendix, Supplementary Materials and Methods* for details of the statistical analysis). All analyses were performed with the MuMIn version 1.43.6 package (52) in the statistical software R version 3.6.3 (53).

THs Extraction and Dosage. THs were extracted from individuals from *A. percula* new recruits sampled in Kimbe Island, dry frozen (previously euthanized in a 200-mg/l solution of MS-222) following the protocol described in ref. 32. More details are described in *SI Appendix*.

Zebrafish *duox* CRISPR-Cas9. Zebrafish *D. rerio* were reared under standard conditions (28 °C, 14L:10D) and staged according to ref. 54. Embryos Tg(*pnp4a:palm-mcherry*)^{wprt10Tg} expressing membrane-targeted mCherry (55, 56) were injected at the one-cell stage with Alt-R CRISPR-Cas9 (36) targeting *duox* and reared on a TH-free diet of brine shrimp and marine rotifers (21). Images of *duox* AltR-injected fish and uninjected controls were acquired on a Zeiss Axio Observer inverted microscope equipped with a Yokogawa CSU-X1M5000 laser spinning disk with Hamamatsu ORCA-Flash 4.0 camera. Regions of interest were defined by the anterior and posterior margin of the anal fin, and proportional coverage of dense interstripe iridophores relative to this region of interest were analyzed using ImageJ software. Numbers of completed or developing interstripes were scored qualitatively. Display levels were adjusted and inverted for visualization in Adobe Photoshop 2021.

Data Availability. All study data are included in the article and/or *SI Appendix*.

ACKNOWLEDGMENTS. This study was supported by Agence Nationale de la Recherche (ANR-19-CE34-0006-Manini and ANR-19-CE14-0010-SENSO) as well as by National Institute of Science (NIH R35 GM122471). We thank Valentin Logeux, Remi Pillot, Nancy Trouillard, and Pascal Romans from the Aquariology Service at Observatoire Océanologique de Banyuls-Sur-Mer for expert technical help for clownfish husbandry. We also thank the Centre de Recherches en Cancérologie de Toulouse (CRCT UMR 1037 INSERM, Plateau Génomique et Transcriptomique) for the nanostring experiments. We thank Marcela Herrera Sarrias for the constructive remarks on the manuscript.

1. M. J. West-Eberhard, Developmental plasticity and the origin of species differences. *Proc. Natl. Acad. Sci. U.S.A.* **102** (suppl. 1), 6543–6549 (2005).
2. O. Leimar, Environmental and genetic cues in the evolution of phenotypic polymorphism. *Evol. Ecol.* **23**, 125–135 (2009).
3. B. Taborsky, *Developmental Plasticity: Preparing for Life in a Complex World* (Elsevier Ltd, 2017).
4. D. W. Pfennig *et al*., Phenotypic plasticity's impacts on diversification and speciation. *Trends Ecol. Evol.* **25**, 459–467 (2010).
5. H. F. Nijhout, Development and evolution of adaptive polyphenisms. *Evol. Dev.* **5**, 9–18 (2003).
6. E. Hammill, A. Rogers, A. P. Beckerman, Costs, benefits and the evolution of inducible defences: A case study with Daphnia pulex. *J. Evol. Biol.* **21**, 705–715 (2008).
7. S. S. Kulkarni, R. J. Denver, I. Gomez-Mestre, D. R. Buchholz, Genetic accommodation via modified endocrine signalling explains phenotypic divergence among spadefoot toad species. *Nat. Commun.* **8**, 993 (2017).
8. S. F. Gilbert, Mechanisms for the environmental regulation of gene expression: Ecological aspects of animal development. *J. Biosci.* **30**, 65–74 (2005).
9. N. Aubin-Horth, S. C. Renn, Genomic reaction norms: Using integrative biology to understand molecular mechanisms of phenotypic plasticity. *Mol. Ecol.* **18**, 3763–3780 (2009).
10. S. F. Gilbert, D. Epel, *Ecological Developmental Biology: The Environmental Regulation of Development, Health and Evolution* (Sinauer Associates, 2015), pp. 576.
11. A. C. Price, C. J. Weadick, J. Shim, F. H. Rodd, Pigments, patterns, and fish behavior. *Zebrafish* **5**, 297–307 (2008).
12. P. D. Dijkstra *et al*., The melanocortin system regulates body pigmentation and social behaviour in a colour polymorphic cichlid fish. *Proc. Biol. Sci.* **284**, 20162838 (2017).
13. Z. W. Culumber, Variation in the evolutionary integration of melanism with behavioral and physiological traits in Xiphophorus variatus. *Evol. Ecol.* **30**, 9–20 (2016).
14. L. Jacquin *et al*., Melanin in a changing world: brown trout coloration reflects alternative reproductive strategies in variable environments. *Behav. Ecol.* **28**, 1423–1434 (2017).
15. F. Cortesi *et al*., Phenotypic plasticity confers multiple fitness benefits to a mimic. *Curr. Biol.* **25**, 949–954 (2015).
16. V. Laudet, The origins and evolution of vertebrate metamorphosis. *Curr. Biol.* **21**, R726–R737 (2011).
17. S. K. McMenamin, D. M. Parichy, Metamorphosis in teleosts. *Curr. Top. Dev. Biol.*. **103**, 127–165 (2013).
18. M. A. Campinho, Teleost metamorphosis: The role of thyroid hormone. *Front. Endocrinol. (Lausanne)* **10**, 383 (2019).
19. S. C. Lema, Hormones, developmental plasticity, and adaptive evolution: Endocrine flexibility as a catalyst for 'plasticity-first' phenotypic divergence. *Mol. Cell. Endocrinol.* **502**, 110678 (2020).
20. L. B. Patterson, D. M. Parichy, Zebrafish pigment pattern formation: Insights into the development and evolution of adult form. *Annu. Rev. Genet.* **53**, 505–530 (2019).
21. S. K. McMenamin *et al*., Thyroid hormone-dependent adult pigment cell lineage and pattern in zebrafish. *Science* **345**, 1358–1361 (2014).
22. L. M. Saunders *et al*., Thyroid hormone regulates distinct paths to maturation in pigment cell lineages. *eLife* **8**, e45181 (2019).
23. G. Litsios *et al*., Mutualism with sea anemones triggered the adaptive radiation of clownfishes. *BMC Evol. Biol.* **12**, 212 (2012).
24. N. Roux, P. Salis, S.-H. Lee, L. Besseau, V. Laudet, Anemonefish, a model for Eco-Evo-Devo. *Evodevo* **11**, 20 (2020).
25. N. Roux *et al*., Staging and normal table of postembryonic development of the clownfish (Amphiprion ocellaris). *Dev. Dyn.* **248**, 545–568 (2019).
26. P. Salis *et al*., Ontogenetic and phylogenetic simplification during white stripe evolution in clownfishes. *BMC Biol.* **16**, 90 (2018).
27. K. Chopra, S. Ishibashi, E. Amaya, Zebrafish *duox* mutations provide a model for human congenital hypothyroidism. *Biol. Open* **8**, bio037655 (2019).
28. O. C. Salles *et al*., First genealogy for a wild marine fish population reveals multigenerational philopatry. *Proc. Natl. Acad. Sci. U.S.A.* **113**, 13245–13250 (2016).
29. P. Salis *et al*., Developmental and comparative transcriptomic identification of iridophore contribution to white barring in clownfish. *Pigment Cell Melanoma Res.* **32**, 391–402 (2019).
30. T. Lorin, F. G. Brunet, V. Laudet, J.-N. Volff, Teleost fish-specific preferential retention of pigmentation gene-containing families after whole genome duplications in Vertebrates. *G3 (Bethesda)* **8**, 1795–1806 (2018).
31. I. Braasch, F. Brunet, J.-N. Volff, M. Schartl, Pigmentation pathway evolution after whole-genome duplication in fish. *Genome Biol. Evol.* **1**, 479–493 (2009).
32. G. Holzer *et al*., Fish larval recruitment to reefs is a thyroid hormone-mediated metamorphosis sensitive to the pesticide chlorpyrifos. *eLife* **6**, e27595 (2017).

33. Y. Inui, S. Miwa, Thyroid hormone induces metamorphosis of flounder larvae. *Gen. Comp. Endocrinol.* **60**, 450–454 (1985).
34. S. Remaud *et al*., Transient hypothyroidism favors oligodendrocyte generation providing functional remyelination in the adult mouse brain. *eLife* **6**, e29996 (2017).
35. J.-S. Park *et al*., Targeted knockout of duox causes defects in zebrafish growth, thyroid development, and social interaction. *J. Genet. Genomics* **46**, 101–104 (2019).
36. K. Hoshijima *et al*., Highly efficient CRISPR-Cas9-based methods for generating deletion mutations and F0 embryos that lack gene function in zebrafish. *Dev. Cell* **51**, 645–657.e4 (2019).
37. D. Gur *et al*., In situ differentiation of iridophore crystallotypes underlies zebrafish stripe patterning. *Nat. Commun.* **11**, 6391 (2020).
38. J. G. Eales, The influence of nutritional state on thyroid function in various vertebrates. *Am. Zool.* **28**, 351–362 (1988).
39. D. S. MacKenzie, C. M. VanPutte, K. A. Leiner, Nutrient regulation of endocrine function in fish. *Aquaculture* **161**, 3–25 (1998).
40. K. A. Leiner, D. S. Mackenzie, Central regulation of thyroidal status in a teleost fish: Nutrient stimulation of T4 secretion and negative feedback of T3. *J. Exp. Zoolog. A Comp. Exp. Biol.* **298**, 32–43 (2003).
41. M. Milenkovic *et al*., Duox expression and related H2O2 measurement in mouse thyroid: Onset in embryonic development and regulation by TSH in adult. *J. Endocrinol.* **192**, 615–626 (2007).
42. A. M. Nedosyko, J. E. Young, J. W. Edwards, K. Burke da Silva, Searching for a toxic key to unlock the mystery of anemonefish and anemone symbiosis. *PLoS One* **9**, e98449 (2014).
43. T. A. Militz, M. I. McCormick, D. S. Schoeman, J. Kinch, P. C. Southgate, Frequency and distribution of melanistic morphs in coexisting population of nine clownfish species in Papua New Guinea. *Mar. Biol.* **163**, 200 (2016).
44. A. L. Ducrest, L. Keller, A. Roulin, Pleiotropy in the melanocortin system, coloration and behavioural syndromes. *Trends Ecol. Evol.* **23**, 502–510 (2008).
45. K. Hayashi, K. Tachihara, J. D. Reimer, Patterns of coexistence of six anemonefish species around subtropical Okinawa-jima Island, Japan. *Coral Reefs* **37**, 1027–1038 (2018).
46. P. Salis, T. Lorin, V. Laudet, B. Frédérich, Magic traits in magic fish: Understanding color pattern evolution using reef fish. *Trends Genet.* **35**, 265–278 (2019).
47. H. Dong *et al*., Transient maternal hypothyroxinemia potentiates the transcriptional response to exogenous thyroid hormone in the fetal cerebral cortex before the onset of fetal thyroid function: A messenger and MicroRNA profiling study. *Cereb. Cortex* **25**, 1735–1745 (2015).
48. M. L. Berumen *et al*., Otolith geochemistry does not reflect dispersal history of clownfish larvae. *Coral Reefs* **29**, 883–891 (2010).
49. K. P. Burnham, D. R. Anderson, *Model Selection and Multimodel Inference* (Springer-Verlag New York, 2002).
50. M. R. E. Symonds, A. Moussalli, A brief guide to model selection, multimodel inference and model averaging in behavioural ecology using Akaike's information criterion. *Behav. Ecol. Sociobiol.* **65**, 13–21 (2011).
51. H. Schielzeth, Simple means to improve the interpretability of regression coefficients. *Methods Ecol. Evol.* **1**, 103–113 (2010).
52. K. Bartoń, MuMIn: Multi-Model Inference. R Package Version 1.43.6 (2019). https://cran.r-project.org/web/packages/MuMIn/index.html. Accessed 10 May 2021.
53. R Core Team, *R: A Language and Environment for Statistical Computing* (R A Lang. Environ. Stat. Comput. R Found. Stat. Comput, Vienna, Austria, 2020).
54. D. M. Parichy, M. R. Elizondo, M. G. Mills, T. N. Gordon, R. E. Engeszer, Normal table of postembryonic zebrafish development: Staging by externally visible anatomy of the living fish. *Dev. Dyn.* **238**, 2975–3015 (2009).
55. D. S. Eom, E. J. Bain, L. B. Patterson, M. E. Grout, D. M. Parichy, Long-distance communication by specialized cellular projections during pigment pattern development and evolution. *eLife* **4**, e12401 (2015).
56. J. E. Spiewak *et al*., Evolution of Endothelin signaling and diversification of adult pigment pattern in Danio fishes. *PLoS Genet.* **14**, e1007538 (2018).

Supplementary Information for:

Thyroid hormones regulate the formation and environmental plasticity of white bars in clownfishes

Pauline Salis[a,b], Natacha Roux[a], Delai Huang[d,e], Anna Marcionetti[f], Pierick Mouginot[b,c], Mathieu Reynaud[g], Océane Salles[b,c], Nicolas Salamin[f], Benoit Pujol[b,c], David M. Parichy[d,e], Serge Planes[b,c], Vincent Laudet[g,h,1]

[a]Observatoire Océanologique de Banyuls-sur-Mer, UMR CNRS 7232 BIOM, Sorbonne Université Paris, 66650 Banyuls-sur-Mer, France ;

[b]Ecole Pratique des Hautes Etudes, Paris Siences et Lettres Research University, Université de Perpignan Via Domitia, CNRS, USR 3278 Centre de Recherches Insulaires et Observatoire de l'environnement, F-66360 Perpignan, France ;

[c]Laboratoire d'Excellence "CORAIL", F-66360 Perpignan, France ;

[d]Department of Biology, University of Virginia, Charlottesville, Virginia 22903;

[e]Department of Cell Biology, University of Virginia, Charlottesville, Virginia 22903;

[f]Department of Computational Biology, University of Lausanne, 1015, Lausanne, Switzerland

[g]Marine Eco-Evo-Devo unit, Okinawa Institute of Science and Technology, Onna son, Okinawa 904-0495 Japan;

[h]Marine Research Station, Institute of Cellular and Organismic Biology, Academia Sinica, 23-10, Dah-Uen Rd, Jiau Shi, I-Lan 262, Taïwan

[1]To whom correspondence may be addressed. Email: vincent.laudet@oist.jp.

This PDF File includes:

Supplementary Materials and Methods

Supplementary Figures S1 to S4

Supplementary Tables 1 to 6

References for SI

Supplementary Materials and Methods

A. ocellaris larval rearing and ethics

A. ocellaris were maintained at 26 °C in separate 60-L aquaria. Breeding pairs laid egg clutches on the underside of a terracotta pot placed in their aquarium. On the night of hatching (9 days post laying, 26 °C), egg clutches were transferred from the parental aquarium to a 30-L larval rearing aquarium. Larvae were fed rotifers (*Brachionus plicatilis*) at 10 individuals per milliliter three times a day for the first 7 days. The ratio of *Artemia nauplii* to rotifers was increased each day until larvae were fed only five individuals of *Artemia nauplii* per milliliter from day 7.

RNA extraction and Transcriptomic analysis of *Amphiprion ocellaris* post embryonic developmental stages

Larvae of *Amphiprion ocellaris* were sampled, euthanized in a MS222 solution (200 mg/l), photographed and conserved in RNAlater prior to RNA extraction. Total RNA was extracted from *A. ocellaris* larvae using Maxwell® 16 Tissue LEV Total RNA Purification Kit (Promega-AS1220) and eluted into 40 ul of RNAse free water. RNA-Seq libraries and sequencing were performed on an Illumina HiSeq4000 sequencer using a stranded protocol as Paired-end 100 base reads.

The raw reads were mapped against *A. ocellaris* reference transcriptome (Ensembl release 98 with the addition of two missing transcripts coding for clec19a--like and gpnmb) using Salmon (v.1.1.0;(1)) Raw counts for each gene were obtained with tximport (v.1.14.2; (2)). Raw counts were normalized to account for differences in sequencing depth and transformed with functions estimateSizeFactor and varianceStabilizingTransformation from the DESeq2 package (v.1.26; (3)).

Principal Component Analyses (PCA) of sample expression levels are performed with gene signals centered but not scaled (using function prcomp from package stats). When displayed, gene coordinates correspond to these genes correlations with the presented components. Only genes that contribute most to the components are displayed.

Transcriptomic analysis of *Amphiprion percula* new recruits

We removed potential adapter contaminations and trimmed the resulting raw reads with cutadapt (v.1.13; (4)) and sickle (v1.29, (5)), respectively. The processed reads were mapped against A. percula reference genome (Ensembl ID: GCA_003047355.1; (6)) using HiSat2 (v.2.1.0; (7)). Raw counts for each gene were obtained with HTSeq (htseq-count, v.0.9.1; (8)), using the available gene annotation of the *A. percula* reference genome. Raw counts were

normalized to account for differences in sequencing depth with the function calcNormFactors (method "TMM") from EdgeR package (v.3.16.5; (9)). Differential expression analysis was performed following the voom pipeline (10) within the limma R package (v.3.30.13; (11)), contrasting the gene expression of recruits from S. gigantea against the ones from H. magnifica. We identified significant differentially expressed genes with the functions decideTests and topTable ("separate" method, p-value adjust method "fdr", log2-fold-change threshold of 1) from the limma package (9).

Drug treatment of *A. ocellaris* larvae

T3 (3,3',5-Triiodo-L-thyronine) and IOP (Iopanoic Acid) were both diluted in dimethyl sulfoxide (T3: T2877, IOP: 14131, DMSO: D8418; Sigma-Aldrich Louis, MI, USA) to a final concentration 1 mM. Methimazole, Potassium Perchlorate and IOP (Methimazole: M8506, Potassium perchlorate 460494, Sigma-Aldrich Louis, MI, USA) were also diluted in DMSO to a respective final concentration of 100 mM, 10 mM and 1 mM. Larvae were treated from 5 until 18 days post hatching in 0.005% DMSO with T3+IOP at 10^{-6}, 10^{-7} and 10^{-8} M (respective dilutions of 1/1000, 1/10000 or 1/100000) or MPI (dilution of 1/1000) or without (controls). For each condition, five larvae were treated in 500-mL fish medium in a beaker. Each day, 100 mL of solution were changed.

Nanostring gene expression analysis

400 ng of total RNA were analyzed using the Nanostring Counter. Each sample was analyzed in a separate multiplexed reaction including eight negative probes and six serial concentrations of positive control probes. Data were imported into nSolver software (version 2.5) for quality checking and data normalization of data according to NanoString analysis guidelines. Analysis was done using the R package TTCA1 (R version 3.5.1).

Life-history characteristics of self-recruiters and immigrants

Right sagittal otoliths were removed from the 218 *A. percula* new-recruits to characterize their age. Otholiths were cleaned, placed in thermoplastic glue on a microscope slide and polished following the Raventos and Macpherson method (12). Otolith measurements were performed using a Zeiss microscope connected to a digital camera and image analysis system. We counted daily rings of each otolith corresponding to the age (in days) at the sampling of each fish.

Statistical analysis of the effect of ecological factors on the number of bars in new recruits

At the time of the sampling in Kimbe bay (5°12′22.56″ S, 150°22′35.58″ E), West New Britain Province, Papua New Guinea, we characterized the new recruit size, age (see Supp Methods) ecological variables (geographic zone, primary host anemone species, depth), and the social structure of the new recruits within its sea anemone (total number of conspecifics inhabiting the sea anemone, size difference between the new recruit and the last subadult in the social hierarchy, female size).

We built quadratic regression models of the number of bars as a response variable depending upon either size or age (not simultaneously because they were strongly correlated; Pearson's correlation coefficient: r = 0.73, N = 218, t = 15.701, p-value < 2.2e-16), their squared value, and ecological and social structure independent variables.

To assess what factors affect the number of bars on new recruits, we followed a multi-model inference approach (13). For each full model (including either age or size), we considered all plausible candidate models and performed a model selection analysis. For each candidate model, we calculated its adjusted R2, its AICc value and its Akaike weight. Models were ranked according their AICc value, with models with the lowest AICc value considered the best (13, 14). To estimate each predictor's contribution, we performed model averaging analyses on each set of candidate models. For each predictor, we calculated its full model averaged parameter estimate β (14) flanked by its 85% confidence interval (15). Predictors were centered and standardized to compare their relative contribution on a common scale, but for the number of conspecifics that was centered (16). The evaluation of a predictor's contribution results in parameter estimates for which the first level of a factor is set as a reference. We interpreted predictors whose confidence interval included zero as uncertain.

Thyroid hormones extraction and dosage of *A. percula* new recruits

TH were extracted from individuals from *A. percula* new recruits sampled in Kimbe Island, dry-frozen (previously euthanized in a 200 mg/l solution of MS-222) following the protocol developed by (17) and adapted from previous TH extractions of teleost fishes (18–20). Briefly, larvae are weighted, crushed in 500 µl of Methanol with a FastPrep 24, centrifuged at 4°C for 10 minutes. Supernatants were collected and reserved. This step was conducted twice and supernatants were pooled. Then, the pellets were resuspended in a mix of methanol (300µl), chloroform (100 µl) and barbital buffer (150 µl), crushed, centrifuged at 4°C and supernatants were collected and reserved with the previous supernatants. Pooled supernatants were dried at 65°C. Hormones were then re-extracted with a mix of methanol, chloroform and barbital buffer twice from the dried extract, centrifuged and supernatant were pooled and dried at 65°C. Final extracts were re-suspended in 250 µl of Phosphate Buffer Saline (PBS) and kept at -

20°C until measurements. TH concentrations were measured by a medical laboratory of Perpignan (Médipole) using an ELISA kit (Access Free T3, T4, Beckman Coulter).

Zebrafish *duox* CRISPR-Cas9

Zebrafish *D. rerio* were reared under standard conditions (28 °C, 14L:10D) and staged according to (21). Embryos Tg(*pnp4a:palm-mcherry*)^{wprt10Tg} expressing membrane-targeted mCherry (mem-Cherry) (22, 23) were injected at the one-cell stage with Alt-R CRISPR-Cas9 (24) targeting *duox*, and reared on a thyroid hormone free diet of brine shrimp and marine rotifers (25). Images of *duox* AltR-injected fish and uninjected controls were acquired on a Zeiss Axio Observer inverted microscope equipped with a Yokogawa CSU-X1M5000 laser spinning disk with Hamamatsu ORCA-Flash 4.0 camera. Regions of interest were defined by the anterior and posterior margin of the anal fin, and proportional coverage of dense interstripe iridophores relative to this region of interest were analyzed using ImageJ software. Numbers of completed or developing interstripes were scored qualitatively. Display levels were adjusted and inverted for visualization in Adobe Photoshop 2021.

Supplementary Figures

A

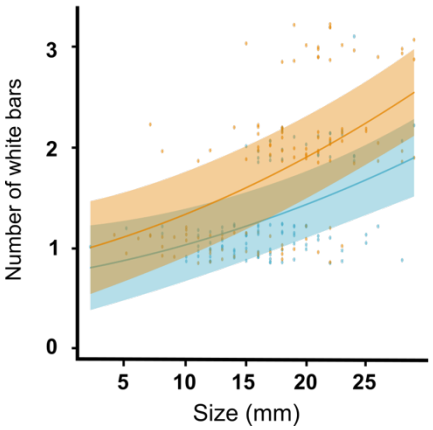

B

	H. magnifica		*S. gigantea*	
Parameter	**Averaged β**	**85% C.I.**	**Averaged β**	**85% C.I.**
Intercept	1.287	1.215; 1.359	**1.582**	**1.472; 1.693**
Size	0.103	0.001; 0.357	0.188	0.088; 0.525
Size2	0.105	0.005; 0.357	0.164	0.051; 0.531
N_Fish	-0.026	-0.181; 0.037	-0.049	-0.218; 0.013
Female size	0.013	-0.026; 0.105	-0.06	-0.185; -0.014
Length difference	0.011	-0.049; 0.118	0.159	0.084; 0.26
Depth	-0.002	-0.073; 0.056	0.002	-0.065; 0.078
Lagoon2	-0.018	-0.257; 0.04	0.521	0.341; 0.701
Lagoon3	-0.01	-0.221; 0.099	0.145	-0.027; 0.318

Figure S1. Formation of white bars of *A. percula* new recruits is differentially influenced by size depending on the anemone species. (**A**) Full model averaged estimates (85% CI) of linear regression parameters from models including age for each anemone species. Blue and orange represent respectively *A. percula* new recruits sampled in *H. magnifica* and in *S. gigantea*. Parameter estimates after model averaging of treatment were compared with "Lagoon 1" as reference for the geographic zone. A parameter estimate whose 85% CI includes zero is considered uncertain and parameter estimates whose 85% CI do not overlap are considered different. (**B**) Full model averaged estimates (85% CI) of linear regression parameters from models including size for each anemone species. Parameter estimates after model averaging of treatment were compared with "Lagoon 1" as reference for the geographic zone. A parameter estimate whose 85% CI includes zero is considered uncertain and parameter estimates whose 85% CI do not overlap are considered different.

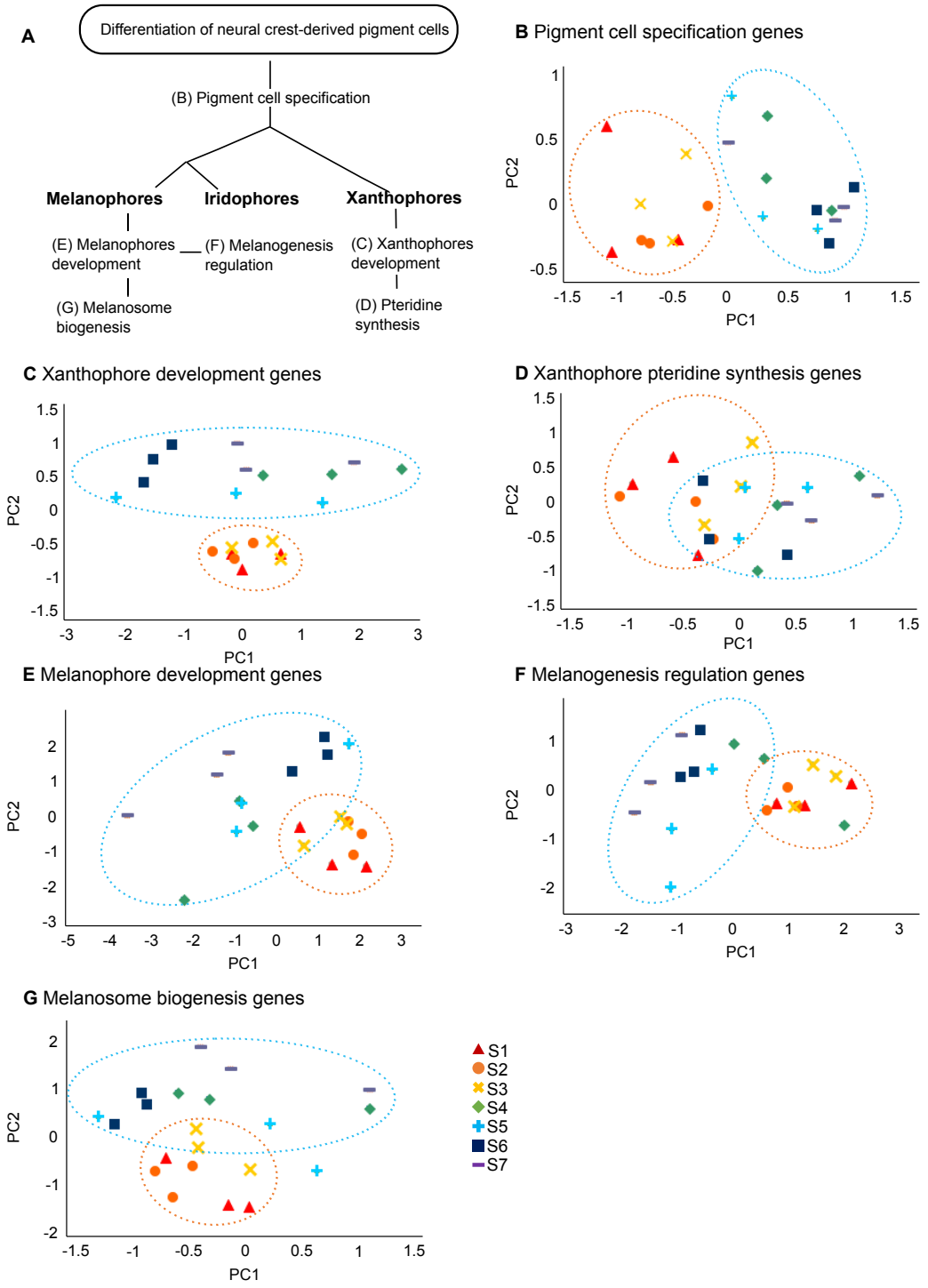

Figure S2. Adult color pattern formation is linked to a switch in expression of pigmentation genes during post-embryonic development. (**A**) Classification of vertebrate pigmentation genes according to functions and cell types (bold). Functional classification within

melanophores and xanthophores is adapted from (26, 27). (**B to G**) Principal component analysis (PCA) of expression of the pigment cell specification genes (**B**), xanthophores developmental genes (**C**), xanthophores pteridine synthesis genes (**D**), melanophores developmental genes (**E**), melanogenesis regulation genes (**F**), melanosome biogenesis genes (**G**). Expressions of genes were extracted from transcriptomic analysis over clownfish stages. All PCA exhibit a clear separation between stage 1 to 3 and stage 4 to 7. The ellipses were arbitrarily drawn around arrays to help resolution: stages 1 to 3 (orange) and 4 to 7 (blue) arrays. All stages had 3 replicates.

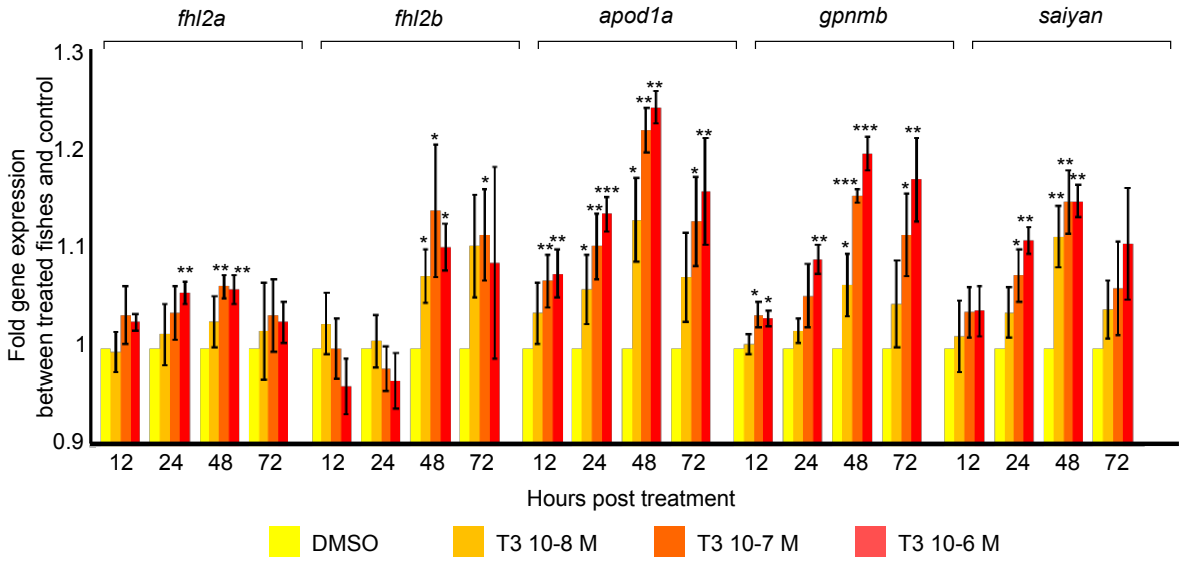

Figure S3. Iridophore genes expressions are modified after T3 treatments. Histogram showing expression of iridophore genes *apod1.a*, *saiyan*, *gpnmb*, *fhl2a* and *fhl2b* in stage 3 larvae treated with DMSO (control- yellow), T3 at 10^{-8} M (light orange), 10^{-7} M (dark orange), 10^{-6} M (red) during 12 hours post-treatment (hpt), 24 hpt, 48 hpt and 72 hpt. (Statistical differences were made between treated larvae and DMSO control larvae: * p-value≤0,05; ** p-value≤0,01; *** p-value≤0,001).

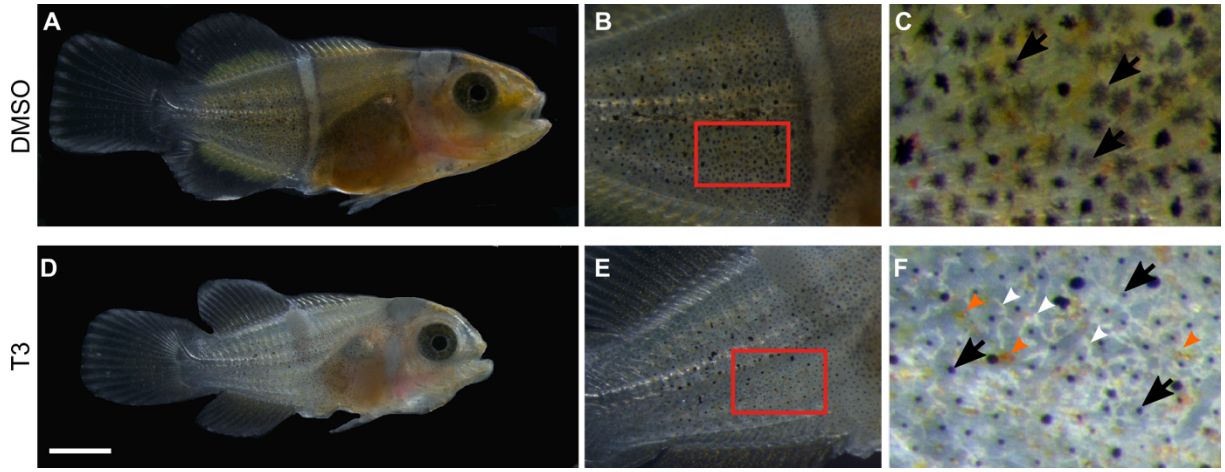

Figure S4. Treatments with thyroid hormones lead to ectopic iridophores over the body and uncomplete white bars. (**A-F**) Stereomicroscope images of stage 3 larvae treated in T3 10^{-6} M (**D-F**) and control larvae (**A-C**) for 9 days. **C** and **F** show higher magnification of larvae. T3 treated juveniles are whiter than controls overall (compare **A** to **D**). Black arrows indicate melanophores, orange arrowheads indicate xanthophores and white arrowheads indicate iridophores. Scale bar corresponds to 1mm.

Supplementary Tables

Table S1: Up to 28 % of the total variance in the number of bars of new recruits is explained by the full model including age in *H. magnifica*. 95% confidence set of best-ranked models examining how the number of bars is affected by age and ecological and social structure variables. For each candidate model, we calculated the log-likelihood, the AICc, the AICc difference with the best ranked model (Delta) according to the model's Akaike weight and the adjusted R^2. "Int" stands for intercept.

Int	Lagoon	Age	Age^2	Depth	Length difference	N Fish	Female size	df	logLik	AICc	delta	weight	$adjR^2$
+			+					3	-58.83	123.9	0	0.1	0.24
+		+						3	-59.25	124.74	0.84	0.06	0.231
+			+			+		4	-58.28	124.97	1.07	0.06	0.252
+			+				+	4	-58.39	125.18	1.28	0.05	0.249
+		+				+		4	-58.52	125.44	1.54	0.04	0.247
+			+		+			4	-58.77	125.94	2.04	0.03	0.241
+			+			+	+	5	-57.67	125.95	2.04	0.03	0.265
+			+	+				4	-58.79	125.98	2.08	0.03	0.241
+		+	+					4	-58.83	126.06	2.16	0.03	0.24
+		+					+	4	-58.86	126.13	2.23	0.03	0.239
+		+				+	+	5	-57.95	126.51	2.61	0.03	0.259
+		+			+			4	-59.08	126.56	2.66	0.03	0.235
+		+		+				4	-59.22	126.84	2.94	0.02	0.232
+			+		+	+	+	6	-57.02	126.9	3	0.02	0.278
+			+		+	+		5	-58.18	126.97	3.07	0.02	0.254
+			+	+		+		5	-58.24	127.08	3.18	0.02	0.253
+		+	+			+		5	-58.26	127.13	3.23	0.02	0.252
+			+	+			+	5	-58.32	127.25	3.35	0.02	0.251
+			+		+		+	5	-58.38	127.38	3.48	0.02	0.25
+		+	+				+	5	-58.39	127.39	3.49	0.02	0.249
+		+			+	+		5	-58.48	127.57	3.67	0.02	0.248
+		+		+		+		5	-58.49	127.59	3.69	0.02	0.247
+		+			+	+	+	6	-57.48	127.82	3.92	0.01	0.269
+			+	+	+			5	-58.7	128.01	4.11	0.01	0.243
+			+	+		+	+	6	-57.58	128.03	4.13	0.01	0.267
+		+	+		+			5	-58.75	128.12	4.22	0.01	0.242
+		+	+			+	+	6	-57.66	128.18	4.28	0.01	0.265
+		+	+	+				5	-58.79	128.19	4.29	0.01	0.241
+		+			+		+	5	-58.8	128.21	4.31	0.01	0.241
+		+		+			+	5	-58.8	128.22	4.32	0.01	0.241
+	+		+					5	-58.81	128.23	4.33	0.01	0.24
+		+		+		+	+	6	-57.88	128.63	4.73	0.01	0.26
+		+		+	+			5	-59.01	128.63	4.73	0.01	0.236
+	+	+						5	-59.22	129.06	5.16	0.01	0.231
+		+	+		+	+	+	7	-56.98	129.14	5.24	0.01	0.279
+			+	+	+	+	+	7	-57.01	129.18	5.28	0.01	0.279
+			+	+	+	+		6	-58.16	129.19	5.29	0.01	0.254
+		+	+		+	+		6	-58.17	129.21	5.31	0.01	0.254
+		+	+	+		+		6	-58.22	129.3	5.4	0.01	0.253
+	+		+			+		6	-58.23	129.32	5.42	0.01	0.253
+			+	+	+		+	6	-58.3	129.47	5.57	0.01	0.251
+		+	+	+			+	6	-58.32	129.5	5.6	0.01	0.251
+	+		+				+	6	-58.34	129.54	5.64	0.01	0.251
+		+	+		+		+	6	-58.38	129.63	5.73	0.01	0.25
+	+	+				+		6	-58.44	129.74	5.84	0.01	0.248
+		+		+	+	+		6	-58.46	129.79	5.88	0.01	0.248
+		+		+	+	+	+	7	-57.46	130.09	6.19	0	0.269
+		+	+	+	+			6	-58.69	130.24	6.34	0	0.243
+		+		+	+		+	6	-58.72	130.3	6.4	0	0.242
+		+	+	+		+	+	7	-57.58	130.32	6.42	0	0.267
+	+		+		+			6	-58.74	130.34	6.44	0	0.242
+	+		+			+	+	7	-57.6	130.37	6.47	0	0.266
+	+		+	+				6	-58.78	130.43	6.53	0	0.241

+	+	+	+						6	-58.81	130.48	6.58	0	0.24
+	+	+						+	6	-58.84	130.54	6.64	0	0.24
+	+	+					+	+	7	-57.89	130.94	7.04	0	0.26
+	+	+			+				6	-59.04	130.95	7.05	0	0.235
+	+	+		+					6	-59.2	131.27	7.37	0	0.232
+	+		+		+	+			7	-58.12	131.41	7.51	0	0.255
+		+	+	+	+	+	+		8	-56.97	131.46	7.56	0	0.279
+	+		+		+	+	+		8	-56.97	131.46	7.56	0	0.279
+		+	+	+	+	+			7	-58.16	131.48	7.58	0	0.254
+	+	+	+			+			7	-58.2	131.57	7.67	0	0.253
+	+		+	+		+			7	-58.2	131.57	7.67	0	0.253
+	+		+	+				+	7	-58.29	131.75	7.85	0	0.252
+		+	+	+	+			+	7	-58.3	131.77	7.87	0	0.251
+	+		+		+			+	7	-58.33	131.82	7.92	0	0.251
+	+	+	+					+	7	-58.33	131.84	7.94	0	0.251
+	+	+			+	+			7	-58.39	131.94	8.04	0	0.25
+	+	+		+		+			7	-58.42	132	8.1	0	0.249
+	+	+			+	+	+		8	-57.43	132.37	8.47	0	0.27
+	+		+	+	+				7	-58.69	132.55	8.65	0	0.243
+	+	+	+		+				7	-58.72	132.62	8.72	0	0.242
+	+		+	+		+	+		8	-57.55	132.62	8.72	0	0.267
+	+	+			+		+		7	-58.77	132.7	8.8	0	0.241
+	+	+	+			+	+		8	-57.59	132.7	8.8	0	0.266
+	+	+	+	+					7	-58.78	132.73	8.83	0	0.241
+	+	+		+				+	7	-58.8	132.76	8.86	0	0.241
+	+	+		+	+				7	-58.99	133.15	9.25	0	0.237
+	+	+		+		+	+		8	-57.85	133.22	9.32	0	0.261
+	+	+	+		+	+			8	-58.11	133.74	9.84	0	0.255
+	+		+	+	+	+			8	-58.11	133.74	9.84	0	0.255
+	+	+	+		+	+	+		9	-56.94	133.8	9.9	0	0.28
+	+		+	+	+	+	+		9	-56.97	133.86	9.96	0	0.279
+	+	+	+	+		+			8	-58.18	133.87	9.97	0	0.254
+					+	+	+		5	-61.71	134.03	10.13	0	0.176
+	+		+	+	+			+	8	-58.27	134.06	10.16	0	0.252
+	+	+	+	+				+	8	-58.29	134.09	10.19	0	0.252
+	+	+	+		+			+	8	-58.33	134.17	10.27	0	0.251
+	+	+		+	+	+			8	-58.38	134.27	10.37	0	0.25
+	+	+		+	+	+	+		9	-57.42	134.76	10.86	0	0.27
+	+	+	+	+	+				8	-58.68	134.87	10.97	0	0.243
+	+	+		+	+			+	8	-58.71	134.93	11.03	0	0.243
+	+	+	+	+		+	+		9	-57.55	135.01	11.11	0	0.267
+	+	+	+	+	+	+			9	-58.11	136.13	12.23	0	0.256
+				+	+	+	+		6	-61.67	136.2	12.3	0	0.177
+	+	+	+	+	+	+	+		10	-56.94	136.25	12.35	0	0.28
+	+	+	+	+	+			+	9	-58.27	136.46	12.56	0	0.252
+	+				+	+	+		7	-61.68	138.53	14.63	0	0.177
+					+	+			4	-65.41	139.22	15.31	0	0.089
+	+			+	+	+	+		8	-61.65	140.82	16.92	0	0.177
+						+	+		4	-66.38	141.16	17.26	0	0.065
+				+	+	+			5	-65.32	141.25	17.35	0	0.091
+						+			3	-67.74	141.73	17.82	0	0.03
+									2	-68.91	141.94	18.04	0	0
+								+	3	-67.89	142.02	18.12	0	0.027
+				+			+	+	5	-65.71	142.03	18.13	0	0.081
+				+			+		4	-67.21	142.82	18.92	0	0.044
+				+				+	4	-67.22	142.84	18.94	0	0.044
+					+			+	4	-67.24	142.88	18.98	0	0.043
+				+					3	-68.36	142.96	19.06	0	0.014
+	+				+	+			6	-65.25	143.36	19.46	0	0.093
+					+				3	-68.6	143.44	19.54	0	0.008
+				+	+			+	5	-66.8	144.22	20.32	0	0.054
+				+	+				4	-68.2	144.8	20.9	0	0.018
+	+			+	+	+			7	-65.15	145.48	21.57	0	0.095
+	+					+	+		6	-66.32	145.51	21.61	0	0.066
+	+					+			5	-67.69	146	22.1	0	0.032
+	+								4	-68.91	146.22	22.32	0	0
+	+							+	5	-67.83	146.28	22.38	0	0.028
+	+			+			+	+	7	-65.71	146.58	22.68	0	0.081
+	+			+			+		6	-67.16	147.18	23.28	0	0.045
+	+			+				+	6	-67.17	147.21	23.31	0	0.045
+	+				+			+	6	-67.19	147.25	23.35	0	0.044
+	+			+					5	-68.32	147.26	23.36	0	0.015
+	+				+				5	-68.6	147.81	23.91	0	0.008
+	+			+	+			+	7	-66.75	148.66	24.76	0	0.056
+	+			+	+				6	-68.16	149.18	25.28	0	0.02

Table S2: Up to 56 % of the total variance in the number of bars of new recruits is explained by the full model including age in *S. gigantea*. 95% confidence set of best-ranked models examining how the number of bars is affected by age and ecological and social structure variables. For each candidate model, we calculated the log-likelihood, the AICc, the AICc difference with the best ranked model (Delta) according to the model's Akaike weight and the adjusted R^2. "Int" stands for intercept.

Int	Lagoon	Age	Age2	Depth	Length difference	N Fish	Female size	df	logLik	AICc	delta	weight	adjR2
+	+	+	+			+		7	-86.62	188.29	0	0.25	0.554
+	+	+				+		6	-88.57	189.93	1.64	0.11	0.534
+	+	+	+		+	+		8	-86.39	190.15	1.86	0.1	0.556
+	+	+	+			+	+	8	-86.57	190.52	2.23	0.08	0.554
+	+	+	+	+		+		8	-86.59	190.54	2.25	0.08	0.554
+	+	+			+	+		7	-88.23	191.52	3.23	0.05	0.537
+	+	+		+		+		7	-88.46	191.98	3.69	0.04	0.535
+	+	+	+		+	+	+	9	-86.14	192.02	3.73	0.04	0.558
+	+	+				+	+	7	-88.52	192.09	3.8	0.04	0.534
+	+	+	+	+	+	+		9	-86.31	192.35	4.06	0.03	0.557
+	+	+	+	+		+	+	9	-86.54	192.81	4.52	0.03	0.554
+	+	+			+	+	+	8	-87.91	193.18	4.89	0.02	0.541
+	+	+		+	+	+		8	-88.03	193.42	5.13	0.02	0.539
+	+	+	+		+		+	8	-88.25	193.88	5.59	0.02	0.537
+	+	+			+		+	7	-89.47	194	5.71	0.01	0.524
+	+	+	+	+	+	+	+	10	-86.02	194.18	5.89	0.01	0.56
+	+	+		+		+	+	8	-88.41	194.19	5.9	0.01	0.535
+	+		+			+		6	-90.79	194.37	6.08	0.01	0.51
+	+	+		+	+	+	+	9	-87.63	194.99	6.7	0.01	0.543
+	+	+		+	+		+	8	-88.96	195.29	7	0.01	0.53
+	+	+	+	+	+		+	9	-87.89	195.52	7.23	0.01	0.541
+	+		+		+	+		7	-90.37	195.8	7.51	0.01	0.515
+	+		+	+		+		7	-90.67	196.4	8.11	0	0.512
+	+		+			+	+	7	-90.78	196.61	8.32	0	0.51
+	+		+		+	+	+	8	-90.13	197.63	9.34	0	0.517
+	+		+	+	+	+		8	-90.13	197.64	9.35	0	0.517
+	+		+		+		+	7	-91.63	198.32	10.02	0	0.501
+	+		+	+		+	+	8	-90.66	198.68	10.39	0	0.512
+	+		+	+	+	+	+	9	-89.82	199.37	11.08	0	0.521
+	+		+	+	+		+	8	-91.07	199.51	11.22	0	0.507
+	+	+			+			6	-93.5	199.79	11.5	0	0.48
+	+	+	+		+			7	-92.63	200.31	12.02	0	0.49
+	+	+					+	6	-93.95	200.69	12.4	0	0.475
+	+	+	+				+	7	-92.82	200.71	12.42	0	0.488
+	+	+		+	+			7	-93.04	201.15	12.86	0	0.485
+	+	+	+	+	+			8	-92.29	201.95	13.66	0	0.494
+	+	+		+			+	7	-93.84	202.74	14.45	0	0.477
+	+	+	+	+			+	8	-92.77	202.92	14.63	0	0.489
+	+		+		+			6	-95.19	203.17	14.88	0	0.461
+	+		+	+	+			7	-94.68	204.43	16.13	0	0.467
+	+		+				+	6	-96.16	205.11	16.82	0	0.45
+	+					+		5	-97.36	205.27	16.98	0	0.435
+	+	+						5	-97.77	206.09	17.8	0	0.43
+	+				+	+		6	-96.83	206.44	18.15	0	0.442
+	+	+	+					6	-96.95	206.69	18.4	0	0.44
+	+					+	+	6	-97.13	207.05	18.76	0	0.438
+	+		+	+			+	7	-96.03	207.11	18.82	0	0.451
+	+			+		+		6	-97.36	207.5	19.21	0	0.435
+	+	+		+				6	-97.67	208.13	19.83	0	0.431
+	+			+	+	+		7	-96.8	208.65	20.36	0	0.442
+	+				+	+	+	7	-96.81	208.67	20.38	0	0.442
+	+	+	+	+				7	-96.91	208.87	20.58	0	0.441
+	+			+		+	+	7	-97.13	209.32	21.03	0	0.438
+		+	+			+		5	-99.38	209.32	21.03	0	0.41
+	+		+					5	-99.52	209.59	21.3	0	0.409

+		+	+			+	+	6	-98.84	210.46	22.17	0	0.417	
+		+				+		4	-101.18	210.73	22.44	0	0.387	
+	+			+	+	+	+	8	-96.78	210.93	22.64	0	0.442	
+		+	+	+		+		6	-99.13	211.04	22.75	0	0.413	
+		+	+		+	+		6	-99.23	211.24	22.95	0	0.412	
+		+	+		+	+	+	7	-98.14	211.33	23.04	0	0.426	
+	+		+	+				6	-99.4	211.58	23.29	0	0.41	
+		+				+	+	5	-100.61	211.77	23.48	0	0.395	
+		+			+	+	+	6	-99.68	212.14	23.85	0	0.407	
+		+	+	+		+	+	7	-98.61	212.28	23.99	0	0.42	
+		+			+	+		5	-100.93	212.42	24.13	0	0.391	
+		+		+		+		5	-101.06	212.68	24.39	0	0.389	
+	+				+		+	6	-100.08	212.94	24.65	0	0.401	
+		+	+	+	+	+		7	-99.04	213.14	24.84	0	0.415	
+		+			+		+	5	-101.3	213.16	24.87	0	0.386	
+		+	+		+		+	6	-100.26	213.3	25.01	0	0.399	
+		+	+	+	+	+	+	8	-98.06	213.49	25.2	0	0.427	
+		+		+		+	+	6	-100.51	213.8	25.51	0	0.396	
+		+		+	+	+	+	7	-99.67	214.4	26.11	0	0.407	
+		+		+	+	+		6	-100.87	214.52	26.23	0	0.391	
+			+			+		4	-103.21	214.79	26.5	0	0.361	
+	+			+	+		+	7	-99.91	214.88	26.59	0	0.404	
+	+				+			5	-102.3	215.15	26.86	0	0.373	
+		+		+	+		+	6	-101.29	215.37	27.08	0	0.386	
+		+	+	+	+		+	7	-100.26	215.57	27.28	0	0.399	
+			+			+	+	5	-102.78	216.12	27.83	0	0.366	
+			+		+	+		5	-102.89	216.33	28.04	0	0.365	
+			+		+	+	+	6	-101.8	216.38	28.09	0	0.379	
+			+	+		+		5	-103.11	216.77	28.48	0	0.362	
+	+			+	+			6	-102.13	217.05	28.76	0	0.375	
+			+		+		+	5	-103.36	217.27	28.98	0	0.359	
+			+	+		+	+	6	-102.7	218.18	29.89	0	0.367	
+			+	+	+	+		6	-102.84	218.47	30.18	0	0.366	
+			+	+	+	+	+	7	-101.79	218.64	30.35	0	0.379	
+			+	+	+		+	6	-103.34	219.46	31.17	0	0.359	
+	+						+	5	-105.48	221.52	33.23	0	0.33	
+		+					+	4	-107.14	222.65	34.36	0	0.306	
+		+	+				+	5	-106.15	222.86	34.57	0	0.32	
+	+							4	-107.47	223.31	35.02	0	0.301	
+	+			+			+	6	-105.48	223.75	35.46	0	0.33	
+						+		3	-109.18	224.57	36.28	0	0.276	
+		+		+			+	5	-107.04	224.64	36.35	0	0.307	
+		+	+	+			+	6	-105.97	224.72	36.43	0	0.323	
+	+			+				5	-107.47	225.5	37.21	0	0.301	
+					+	+		4	-108.75	225.87	37.58	0	0.283	
+				+		+		4	-108.82	226.01	37.72	0	0.282	
+						+	+	4	-109.17	226.71	38.42	0	0.276	
+			+				+	4	-109.31	226.99	38.7	0	0.274	
+				+	+	+		5	-108.52	227.6	39.31	0	0.286	
+					+	+	+	5	-108.58	227.72	39.43	0	0.285	
+		+			+			4	-109.69	227.75	39.46	0	0.269	
+				+		+	+	5	-108.82	228.19	39.9	0	0.282	
+		+	+		+			5	-109.07	228.69	40.4	0	0.278	
+			+	+			+	5	-109.24	229.03	40.74	0	0.275	
+				+	+	+	+	6	-108.39	229.57	41.28	0	0.288	
+		+		+	+			5	-109.69	229.94	41.65	0	0.269	
+			+		+			4	-111.12	230.61	42.32	0	0.247	
+		+	+	+	+			6	-109.05	230.89	42.6	0	0.278	
+					+		+	4	-112.03	232.43	44.14	0	0.233	
+			+	+	+			5	-111.12	232.8	44.51	0	0.247	
+				+	+		+	5	-112	234.56	46.27	0	0.233	
+		+						3	-115.78	237.77	49.48	0	0.172	
+		+	+					4	-115.2	238.76	50.47	0	0.182	
+		+		+				4	-115.57	239.5	51.21	0	0.176	
+		+	+	+				5	-114.89	240.34	52.05	0	0.187	
+			+					3	-117.3	240.82	52.53	0	0.146	
+					+			3	-117.89	241.99	53.7	0	0.136	
+			+	+				4	-117.13	242.63	54.34	0	0.149	
+				+	+			4	-117.82	244.01	55.71	0	0.137	
+							+	3	-119.25	244.73	56.44	0	0.112	
+				+			+	4	-118.82	246.01	57.72	0	0.12	
+								2	-125.24	254.59	66.3	0	0	
+				+				3	-124.69	255.59	67.3	0	0.011	

233

234

Table S3: Up to 30.4 % of the total variance in the number of bars of new recruits is explained by the full model including size in *H. magnifica*. 95% confidence set of best-ranked models examining how the number of bars is affected by age and ecological and social structure variables. For each candidate model, we calculated the log-likelihood, the AICc, the AICc difference with the best ranked model (Delta) according to the model's Akaike weight and the adjusted R^2. "Int" stands for intercept.

Int	Lagoon	Depth	Length difference	N Fish	Size	Size^2	Female size	df	logLik	AICc	delta	weight	adjR^2
+						+		3	-57.7	121.63	0	0.08	0.264
+					+			3	-57.8	121.84	0.21	0.07	0.262
+				+	+			4	-57.08	122.56	0.93	0.05	0.277
+				+		+		4	-57.19	122.78	1.14	0.04	0.275
+			+		+			4	-57.2	122.81	1.17	0.04	0.275
+			+			+		4	-57.28	122.97	1.33	0.04	0.273
+						+	+	4	-57.33	123.06	1.43	0.04	0.272
+					+		+	4	-57.39	123.18	1.54	0.04	0.271
+				+	+		+	5	-56.48	123.57	1.94	0.03	0.29
+					+	+		4	-57.6	123.6	1.97	0.03	0.266
+		+				+		4	-57.66	123.72	2.09	0.03	0.265
+				+		+	+	5	-56.67	123.94	2.31	0.02	0.286
+		+			+			4	-57.79	123.99	2.36	0.02	0.262
+				+	+	+		5	-56.99	124.6	2.97	0.02	0.279
+			+		+		+	5	-57.01	124.63	3	0.02	0.279
+			+	+	+			5	-57.01	124.63	3	0.02	0.279
+		+		+	+			5	-57.07	124.76	3.12	0.02	0.277
+	+					+		5	-57.07	124.76	3.12	0.02	0.277
+			+		+	+		5	-57.07	124.76	3.12	0.02	0.277
+			+			+	+	5	-57.09	124.79	3.16	0.02	0.277
+			+	+		+		5	-57.14	124.9	3.27	0.01	0.276
+		+		+		+		5	-57.15	124.9	3.27	0.01	0.276
+		+	+		+			5	-57.15	124.92	3.29	0.01	0.276
+		+	+			+		5	-57.18	124.97	3.34	0.01	0.275
+					+	+	+	5	-57.22	125.05	3.42	0.01	0.274
+		+				+	+	5	-57.27	125.15	3.51	0.01	0.273
+		+			+		+	5	-57.36	125.34	3.71	0.01	0.271
+	+				+			5	-57.4	125.42	3.79	0.01	0.27
+	+		+			+		6	-56.41	125.69	4.05	0.01	0.291
+				+	+	+	+	6	-56.43	125.72	4.09	0.01	0.291
+			+	+	+		+	6	-56.44	125.75	4.11	0.01	0.29
+		+		+	+		+	6	-56.45	125.77	4.13	0.01	0.29
+		+			+	+		5	-57.58	125.77	4.14	0.01	0.267
+	+			+		+		6	-56.49	125.85	4.22	0.01	0.289
+	+			+	+			6	-56.58	126.03	4.39	0.01	0.288
+	+		+		+			6	-56.59	126.04	4.41	0.01	0.287
+		+		+		+	+	6	-56.59	126.05	4.42	0.01	0.287
+			+	+		+	+	6	-56.61	126.09	4.46	0.01	0.287
+	+					+	+	6	-56.64	126.15	4.52	0.01	0.286
+			+		+	+	+	6	-56.89	126.65	5.01	0.01	0.281
+			+	+	+	+		6	-56.92	126.71	5.08	0.01	0.28
+	+				+		+	6	-56.95	126.76	5.13	0.01	0.28
+		+	+		+		+	6	-56.95	126.77	5.14	0.01	0.28
+		+	+			+	+	6	-56.98	126.82	5.18	0.01	0.279
+		+		+	+	+		6	-56.98	126.82	5.19	0.01	0.279
+		+	+	+	+			6	-56.99	126.84	5.21	0.01	0.279
+		+	+		+	+		6	-57.01	126.88	5.25	0.01	0.279
+	+				+	+		6	-57.04	126.95	5.32	0.01	0.278
+	+	+				+		6	-57.06	126.99	5.36	0.01	0.278
+	+			+		+	+	7	-55.92	127	5.37	0.01	0.301
+		+	+	+		+		6	-57.08	127.02	5.39	0.01	0.277
+	+			+	+		+	7	-55.95	127.06	5.43	0.01	0.301
+		+			+	+	+	6	-57.18	127.22	5.59	0	0.275
+	+		+			+	+	7	-56.22	127.6	5.97	0	0.295
+	+	+			+			6	-57.38	127.63	6	0	0.271
+	+		+		+	+		7	-56.31	127.78	6.15	0	0.293
+	+		+	+		+		7	-56.34	127.85	6.22	0	0.292
+		+		+	+	+	+	7	-56.39	127.95	6.31	0	0.291
+	+			+	+	+		7	-56.39	127.96	6.32	0	0.291

+			+	+	+	+	+	7	-56.4	127.96	6.33	0	0.291
+	+		+		+		+	7	-56.4	127.96	6.33	0	0.291
+	+	+	+			+		7	-56.41	127.99	6.35	0	0.291
+		+	+	+	+		+	7	-56.42	128.01	6.38	0	0.291
+	+		+	+	+			7	-56.44	128.04	6.41	0	0.29
+	+	+		+		+		7	-56.48	128.13	6.5	0	0.29
+	+	+		+	+			7	-56.55	128.27	6.64	0	0.288
+		+	+	+		+	+	7	-56.56	128.29	6.66	0	0.288
+	+	+	+		+			7	-56.58	128.33	6.7	0	0.287
+	+				+	+	+	7	-56.61	128.39	6.76	0	0.287
+	+	+				+	+	7	-56.64	128.45	6.82	0	0.286
+		+	+		+	+	+	7	-56.81	128.79	7.16	0	0.283
+		+	+	+	+	+		7	-56.89	128.94	7.3	0	0.281
+	+	+			+		+	7	-56.94	129.04	7.41	0	0.28
+	+			+	+	+	+	8	-55.8	129.12	7.48	0	0.304
+	+	+			+	+		7	-57.03	129.22	7.59	0	0.278
+	+	+		+		+	+	8	-55.91	129.34	7.71	0	0.301
+	+		+	+		+	+	8	-55.92	129.35	7.71	0	0.301
+	+	+		+	+		+	8	-55.94	129.39	7.76	0	0.301
+	+		+	+	+		+	8	-55.94	129.41	7.77	0	0.301
+	+		+		+	+	+	8	-56.12	129.76	8.13	0	0.297
+	+	+	+			+	+	8	-56.22	129.95	8.31	0	0.295
+	+		+	+	+	+		8	-56.22	129.97	8.33	0	0.295
+	+	+	+		+	+		8	-56.31	130.13	8.49	0	0.293
+	+	+	+	+		+		8	-56.34	130.2	8.56	0	0.292
+		+	+	+	+	+	+	8	-56.37	130.26	8.63	0	0.292
+	+	+		+	+	+		8	-56.37	130.26	8.63	0	0.292
+	+	+	+		+		+	8	-56.4	130.31	8.68	0	0.291
+	+	+	+	+	+			8	-56.43	130.37	8.74	0	0.291
+	+	+			+	+	+	8	-56.61	130.73	9.1	0	0.287
+	+	+		+	+	+	+	9	-55.79	131.5	9.87	0	0.304
+	+		+	+	+	+	+	9	-55.8	131.52	9.88	0	0.304
+	+	+	+	+		+	+	9	-55.91	131.74	10.11	0	0.301
+	+	+	+	+	+		+	9	-55.93	131.78	10.15	0	0.301
+	+	+	+		+	+	+	9	-56.12	132.16	10.53	0	0.297
+	+	+	+	+	+	+		9	-56.22	132.35	10.72	0	0.295
+	+	+	+	+	+	+	+	10	-55.79	133.95	12.32	0	0.304
+			+	+			+	5	-61.71	134.03	12.4	0	0.176
+		+	+	+			+	6	-61.67	136.2	14.56	0	0.177
+	+		+	+			+	7	-61.68	138.53	16.9	0	0.177
+			+	+				4	-65.41	139.22	17.58	0	0.089
+	+	+	+	+			+	8	-61.65	140.82	19.18	0	0.177
+				+			+	4	-66.38	141.16	19.53	0	0.065
+		+	+	+				5	-65.32	141.25	19.61	0	0.091
+				+				3	-67.74	141.73	20.09	0	0.03
+								2	-68.91	141.94	20.31	0	0
+							+	3	-67.89	142.02	20.38	0	0.027
+		+		+			+	5	-65.71	142.03	20.39	0	0.081
+		+		+				4	-67.21	142.82	21.18	0	0.044
+		+					+	4	-67.22	142.84	21.21	0	0.044
+			+				+	4	-67.24	142.88	21.25	0	0.043
+		+						3	-68.36	142.96	21.33	0	0.014
+	+		+	+				6	-65.25	143.36	21.73	0	0.093
+			+					3	-68.6	143.44	21.81	0	0.008
+		+	+				+	5	-66.8	144.22	22.58	0	0.054
+		+	+					4	-68.2	144.8	23.17	0	0.018
+	+	+	+	+				7	-65.15	145.48	23.84	0	0.095
+	+			+			+	6	-66.32	145.51	23.88	0	0.066
+	+			+				5	-67.69	146	24.37	0	0.032
+	+							4	-68.91	146.22	24.58	0	0
+	+						+	5	-67.83	146.28	24.64	0	0.028
+	+	+		+			+	7	-65.71	146.58	24.94	0	0.081
+	+	+		+				6	-67.16	147.18	25.54	0	0.045
+	+	+					+	6	-67.17	147.21	25.58	0	0.045
+	+		+				+	6	-67.19	147.25	25.61	0	0.044
+	+	+						5	-68.32	147.26	25.62	0	0.015
+	+		+					5	-68.6	147.81	26.18	0	0.008
+	+	+	+				+	7	-66.75	148.66	27.02	0	0.056
+	+	+	+					6	-68.16	149.18	27.55	0	0.02

Table S4: Up to 65.6 % of the total variance in the number of bars of new recruits is explained by the full model including size in *S. gigantea*. 95% confidence set of best-ranked models examining how the number of bars is affected by age and ecological and social structure variables. For each candidate model, we calculated the log-likelihood, the AICc, the AICc difference with the best ranked model (Delta) according to the model's Akaike weight and the adjusted R^2. "Int" stands for intercept.

Int	Lagoon	Depth	Length difference	N Fish	Size	Size^2	Female size	df	logLik	AICc	delta	weight	adjR^2
+	+		+		+		+	7	-75.8	166.67	0	0.14	0.652
+	+		+			+	+	7	-75.88	166.83	0.16	0.13	0.652
+	+		+	+	+			7	-76.36	167.78	1.12	0.08	0.648
+	+		+	+		+		7	-76.48	168.02	1.35	0.07	0.647
+	+		+		+	+	+	8	-75.52	168.41	1.74	0.06	0.655
+	+		+	+	+		+	8	-75.59	168.55	1.89	0.05	0.654
+	+		+	+		+	+	8	-75.74	168.85	2.18	0.05	0.653
+	+	+	+		+		+	8	-75.79	168.96	2.3	0.04	0.652
+	+	+	+			+	+	8	-75.88	169.13	2.46	0.04	0.652
+	+		+			+		6	-78.4	169.58	2.92	0.03	0.63
+	+		+	+	+	+		8	-76.14	169.64	2.98	0.03	0.65
+	+	+	+	+	+			8	-76.31	170	3.33	0.03	0.648
+	+		+		+			6	-78.66	170.1	3.43	0.02	0.628
+	+			+	+			6	-78.73	170.24	3.57	0.02	0.628
+	+	+	+	+		+		8	-76.48	170.33	3.66	0.02	0.647
+	+		+	+	+	+	+	9	-75.35	170.44	3.77	0.02	0.656
+	+	+	+		+	+	+	9	-75.52	170.77	4.1	0.02	0.655
+	+	+	+	+	+		+	9	-75.57	170.86	4.2	0.02	0.654
+	+	+	+	+		+	+	9	-75.74	171.21	4.54	0.01	0.653
+	+		+		+	+		7	-78.2	171.45	4.78	0.01	0.632
+	+			+		+		6	-79.45	171.68	5.01	0.01	0.621
+	+	+	+			+		7	-78.39	171.84	5.18	0.01	0.63
+	+	+	+	+	+	+		9	-76.11	171.96	5.29	0.01	0.65
+	+	+		+	+			7	-78.48	172.01	5.35	0.01	0.63
+	+	+	+		+			7	-78.65	172.35	5.69	0.01	0.628
+	+			+	+	+		7	-78.71	172.47	5.81	0.01	0.628
+	+			+	+		+	7	-78.73	172.51	5.85	0.01	0.628
+	+	+	+	+	+	+	+	10	-75.35	172.83	6.16	0.01	0.656
+	+	+		+		+		7	-79.31	173.67	7.01	0	0.622
+	+	+	+		+	+		8	-78.2	173.76	7.1	0	0.632
+	+			+		+	+	7	-79.43	173.92	7.25	0	0.621
+	+	+		+	+	+		8	-78.47	174.31	7.65	0	0.63
+	+	+		+	+		+	8	-78.48	174.33	7.66	0	0.63
+	+			+	+	+	+	8	-78.71	174.79	8.12	0	0.628
+	+	+		+		+	+	8	-79.3	175.96	9.3	0	0.623
+	+	+		+	+	+	+	9	-78.47	176.67	10	0	0.63
+			+			+	+	5	-84.63	179.81	13.14	0	0.573
+			+		+		+	5	-84.91	180.38	13.72	0	0.571
+	+				+		+	6	-83.82	180.43	13.77	0	0.581
+		+	+			+	+	6	-84.39	181.57	14.91	0	0.576
+			+		+	+	+	6	-84.39	181.57	14.91	0	0.576
+		+	+		+		+	6	-84.46	181.7	15.03	0	0.575
+			+	+		+	+	6	-84.54	181.86	15.2	0	0.574
+	+	+			+		+	7	-83.5	182.05	15.39	0	0.584
+			+	+	+		+	6	-84.77	182.32	15.65	0	0.572
+	+					+	+	6	-84.79	182.37	15.7	0	0.572
+	+				+	+	+	7	-83.82	182.69	16.03	0	0.581
+	+				+			5	-86.27	183.09	16.42	0	0.557
+		+	+		+	+	+	7	-84.07	183.19	16.52	0	0.579
+			+	+		+		5	-86.44	183.44	16.78	0	0.555
+		+	+	+	+		+	7	-84.24	183.53	16.87	0	0.577
+		+	+	+		+	+	7	-84.26	183.58	16.92	0	0.577
+			+	+	+	+	+	7	-84.3	183.65	16.99	0	0.576
+			+	+	+			5	-86.67	183.9	17.23	0	0.553
+	+	+				+	+	7	-84.61	184.27	17.61	0	0.573
+	+	+			+	+	+	8	-83.5	184.37	17.7	0	0.584
+	+					+		5	-86.92	184.39	17.72	0	0.551
+		+	+	+	+			6	-85.92	184.62	17.96	0	0.561

+	+	+			+			6	-85.96	184.7	18.03	0	0.56
+		+	+	+		+		6	-85.99	184.76	18.09	0	0.56
+		+	+	+	+	+	+	8	-83.91	185.2	18.53	0	0.58
+	+				+	+		6	-86.22	185.22	18.55	0	0.558
+			+	+	+	+		6	-86.24	185.27	18.6	0	0.557
+		+		+	+			5	-87.55	185.66	19	0	0.544
+				+	+			4	-88.78	185.93	19.26	0	0.532
+	+	+				+		6	-86.74	186.27	19.6	0	0.552
+		+	+	+	+	+		7	-85.65	186.35	19.69	0	0.563
+				+		+		4	-89.21	186.79	20.13	0	0.527
+	+	+			+	+		7	-85.93	186.92	20.25	0	0.561
+		+		+		+		5	-88.29	187.13	20.47	0	0.537
+		+		+	+		+	6	-87.32	187.43	20.76	0	0.547
+				+	+		+	5	-88.54	187.64	20.97	0	0.534
+		+		+	+	+		6	-87.52	187.82	21.16	0	0.545
+				+	+	+		5	-88.68	187.91	21.24	0	0.533
+			+			+		4	-89.79	187.94	21.27	0	0.521
+				+		+	+	5	-89.07	188.69	22.03	0	0.529
+		+		+		+	+	6	-88.15	189.09	22.42	0	0.538
+			+		+			4	-90.49	189.35	22.69	0	0.513
+		+	+			+		5	-89.47	189.5	22.84	0	0.524
+		+		+	+	+	+	7	-87.3	189.65	22.99	0	0.547
+				+	+	+	+	6	-88.46	189.71	23.04	0	0.535
+			+		+	+		5	-89.69	189.93	23.27	0	0.522
+		+	+		+			5	-89.93	190.41	23.74	0	0.52
+		+	+		+	+		6	-89.3	191.39	24.73	0	0.526
+		+			+		+	5	-92.65	195.86	29.2	0	0.49
+					+		+	4	-94.05	196.48	29.81	0	0.474
+		+			+	+	+	6	-92.65	198.09	31.43	0	0.49
+						+	+	4	-94.99	198.36	31.69	0	0.463
+		+				+	+	5	-93.94	198.44	31.78	0	0.475
+					+	+	+	5	-94.03	198.61	31.95	0	0.474
+		+			+			4	-98.01	204.38	37.72	0	0.427
+	+			+				5	-97.36	205.27	38.61	0	0.435
+					+			3	-99.59	205.41	38.74	0	0.408
+		+				+		4	-98.93	206.23	39.57	0	0.416
+	+		+	+				6	-96.83	206.44	39.78	0	0.442
+		+			+	+		5	-97.97	206.5	39.83	0	0.428
+						+		3	-100.14	206.51	39.84	0	0.401
+	+			+			+	6	-97.13	207.05	40.38	0	0.438
+					+	+		4	-99.48	207.32	40.66	0	0.409
+	+	+		+				6	-97.36	207.5	40.84	0	0.435
+	+	+	+	+				7	-96.8	208.65	41.99	0	0.442
+	+		+	+			+	7	-96.81	208.67	42	0	0.442
+	+	+		+			+	7	-97.13	209.32	42.65	0	0.438
+	+	+	+	+			+	8	-96.78	210.93	44.26	0	0.442
+	+		+				+	6	-100.08	212.94	46.28	0	0.401
+	+	+	+				+	7	-99.91	214.88	48.21	0	0.404
+	+		+					5	-102.3	215.15	48.49	0	0.373
+	+	+	+					6	-102.13	217.05	50.38	0	0.375
+	+						+	5	-105.48	221.52	54.86	0	0.33
+	+							4	-107.47	223.31	56.65	0	0.301
+	+	+					+	6	-105.48	223.75	57.09	0	0.33
+				+				3	-109.18	224.57	57.91	0	0.276
+	+	+						5	-107.47	225.5	58.84	0	0.301
+			+	+				4	-108.75	225.87	59.21	0	0.283
+		+		+				4	-108.82	226.01	59.34	0	0.282
+				+			+	4	-109.17	226.71	60.05	0	0.276
+		+	+	+				5	-108.52	227.6	60.93	0	0.286
+			+	+			+	5	-108.58	227.72	61.05	0	0.285
+		+		+			+	5	-108.82	228.19	61.52	0	0.282
+		+	+	+			+	6	-108.39	229.57	62.9	0	0.288
+			+				+	4	-112.03	232.43	65.77	0	0.233
+		+	+				+	5	-112	234.56	67.89	0	0.233
+			+					3	-117.89	241.99	75.32	0	0.136
+		+	+					4	-117.82	244.01	77.34	0	0.137
+							+	3	-119.25	244.73	78.06	0	0.112
+		+					+	4	-118.82	246.01	79.34	0	0.12
+								2	-125.24	254.59	87.92	0	0
+		+						3	-124.69	255.59	88.93	0	0.011

Table S5. List of pigmentation genes studied in the transcriptomic analysis of post-embryonic development in *A. ocellaris*. List of pigmentation genes according to their category. Functional classification is adapted from (26, 27). Accession Ensembl number is given for each gene except gpnmb.

Accession number Ensembl	*gene symbol*	gene name	Category
ENSAOCG00000005144	*cdh2 (ncad)*	cadherin2	Pigment cell specification
ENSAOCG00000014547	*lef1*	lymphoid enhancer-binding factor 1	Pigment cell specification
ENSAOCG00000008125	*ovol1*	ovo-like zinc finger 1a	Pigment cell specification
ENSAOCG00000020607	*wnt3a*	wingless-type MMTV integration site family, member 3A	Pigment cell specification
ENSAOCG00000007456	*csf1ra*	Colony stimulating factor 1 receptor a	Iridophores genes
ENSAOCG00000020586	*ece2b*	Endotheline converting enzyme	Iridophores genes
ENSAOCG00000014365	*ednrb1a / rse**	Endotheline receptor beta a	Iridophores genes
ENSAOCG00000020189	*fhl2a*	four and a half LIM domains 2	Iridophores genes
ENSAOCG00000019397	*fhl2b*	four and a half LIM domains protein 2-like	Iridophores genes
ENSAOCG00000012258	*saiyan*	Unnamed	Iridophores genes
ENSAOCG00000023574	*apod1a*	apolipoprotein d (LOC111565550)	Iridophores genes
	gpnmb	Glycoprotein nmb	Iridophores genes
ENSAOCG00000006661	*foxd3*	Forkhead box D3	Iridophores genes
ENSAOCG00000022720	*gbx2*	gastrulation brain homeobox 2	Iridophores genes
ENSAOCG00000002838	*gart**	codes for : Phosphoribosylglycinamide formyltransferase, phosphoribosylglycinamide synthetase, phosphoribosylaminoimidazole synthetase	Iridophores genes
ENSAOCG00000003292	*gmps*	Guanine monophosphate synthase	Iridophores genes
ENSAOCG00000009335	*impdh1b*	Inosine-5,-monophosphate dehydrogenase 1a	Iridophores genes
ENSAOCG00000023322	*ltk*	Leukocyte receptor tyrosine kinase	Iridophores genes
ENSAOCG00000018274	*med12*	mediator complex subunit 12	Iridophores genes
ENSAOCG00000018820	*MPV17*	mitochondrial protein MPV17	Iridophores genes
ENSAOCG00000001912	*oca2**	oculocutaneous albinism 2	Iridophores genes
ENSAOCG00000004706	*paics**	code for Phosphoribosylaminoimidazole carboxylase and phosphoribosylaminoimidazolesuccinocarboxamide synthase	Iridophores genes
ENSAOCG00000003975	*prkaca*	protein kinase A	Iridophores genes
ENSAOCG00000010603	*pnp4*	purine nucleoside phosphorylase 4a	Iridophores genes
ENSAOCG00000003175	*sox10**	SRY-box 10	Iridophores genes
ENSAOCG00000020276	*sox9**	SRY-box 9	Iridophores genes
ENSAOCG00000016699	*tfap2a**	Transcription factor AP-2 alpha	Iridophores genes
ENSAOCG00000015566	*trim33*	Tripartite motif containing 33	Iridophores genes
ENSAOCG00000020418	*alk*	ALK receptor tyrosine kinase	Iridophores genes

ENSAOCG00000007456	*csf1ra*	Colony stimulating factor 1 receptor a	Xanthophores genes development
ENSAOCG00000011059	*leo1*	LEO1 homolog, Paf1/RNA polymerase II complex component	Xanthophores genes development
ENSAOCG00000004812	*pax3*	Paired box 3	Xanthophores genes development
ENSAOCG00000006771	*pax7*	Paired box 7	Xanthophores genes development
ENSAOCG00000008605	*slc2a11b*	Solute carrier family 2, facilitated glucose transporter member 11-like	Xanthophores genes development
ENSAOCG00000010408	*slc2a15a*	Solute carrier family 2, facilitated glucose transporter member15-like	Xanthophores genes development
ENSAOCG00000021551	*slc2a15b*	Solute carrier family 2, facilitated glucose transporter member15-like	Xanthophores genes development
ENSAOCG00000002370	*sox5*	SRY box5	Xanthophores genes development
ENSAOCG00000007799	*sox5*	SRY box5	Xanthophores genes development
ENSAOCT00000008163	*sox5*	SRY box5	Xanthophores genes development
ENSAOCT00000000918	*sox5*	SRY box5	Xanthophores genes development
ENSAOCG00000003175	*sox10**	SRY-box 10	Xanthophores genes development
ENSAOCG00000002838	*gart**	codes for : Phosphoribosylglycinamide formyltransferase, phosphoribosylglycinamide synthetase, phosphoribosylaminoimidazole synthetase	Xanthophores Pteridine synthesis
ENSAOCG00000012029	*gchfr*	GTP cyclohydrolase I feedback regulator	Xanthophores Pteridine synthesis
ENSAOCG00000004706	*paics**	Phosphoribosylaminoimidazole carboxylase, phosphoribosylaminoimidazole succinocarboxamide synthetase	Xanthophores Pteridine synthesis
ENSAOCG00000004933	*pcbd1*	Pterin-4 alpha-carbinolamine dehydratase/dimerization cofactor of hepatocyte nuclear factor 1 alpha	Xanthophores Pteridine synthesis
ENSAOCG00000022228	*pcbd2*	pterin-4-alpha-carbinolamine dehydratase 2-like	Xanthophores Pteridine synthesis
ENSAOCG00000019937	*pts*	6-pyruvoyl tetrahydrobiopterin synthase-like	Xanthophores Pteridine synthesis
ENSAOCG00000024579	*qdpr*	Quinoid dihydropteridine reductase	Xanthophores Pteridine synthesis
ENSAOCG00000023277	*spr*	sepiapterin reductase	Xanthophores Pteridine synthesis
ENSAOCG00000020158	*xdh*	Xanthine dehydrogenase	Xanthophores Pteridine synthesis
ENSAOCG00000016477	*ankrd27*	Ankyrin repeat domain 27	Melanosome biogenesis
ENSAOCG00000024000	*ap1g1*	Adaptor related protein complex 1 subunit gamma 1	Melanosome biogenesis
ENSAOCG00000004909	*ap1m1*	Adaptor related protein complex 1 subunit mu 1	Melanosome biogenesis
ENSAOCG00000001638	*ap3b1*	adaptor related protein complex 3 subunit beta 1	Melanosome biogenesis
ENSAOCG00000006552	*ap3d1*	Adaptor related protein complex 3 subunit delta 1	Melanosome biogenesis
ENSAOCG00000001801	*arcn1*	archain 1	Melanosome biogenesis
ENSAOCG00000004733	*bloc1s1*	Biogenesis of lysosomal organelles complex 1 subunit 1	Melanosome biogenesis
ENSAOCG00000010905	*bloc1s2*	Biogenesis of lysosomal organelles complex 1 subunit 2	Melanosome biogenesis
ENSAOCG00000022190	*bloc1s3*	Biogenesis of lysosomal organelles complex 1 subunit 3	Melanosome biogenesis
ENSAOCG00000010366	*bloc1s4*	Biogenesis of lysosomal organelles complex 1 subunit 4	Melanosome biogenesis
ENSAOCG00000016530	*bloc1s5*	Biogenesis of lysosomal organelles complex 1 subunit 5	Melanosome biogenesis
ENSAOCG00000022240	*cd63*	CD63 molecule	Melanosome biogenesis
ENSAOCG00000015946	*dtnbp1*	Dystrobrevin binding protein 1	Melanosome biogenesis
ENSAOCG00000005815	*fig4*	FIG4 phosphoinositide 5-phosphatase	Melanosome biogenesis

ENSAOCG00000024048	*gpr143*	G protein-coupled receptor 143	Melanosome biogenesis
ENSAOCG00000022280	*hps3*	https://zfin.org/ZDB-GENE-061110-115	Melanosome biogenesis
ENSAOCG00000018442	*hps5*	https://zfin.org/ZDB-GENE-070410-80	Melanosome biogenesis
ENSAOCG00000023831	*kif13a*	Kinesin family member 13A	Melanosome biogenesis
ENSAOCG00000003276	*lyst*	lysosomal trafficking regulator	Melanosome biogenesis
ENSAOCG00000020231	*mlana*	https://zfin.org/ZDB-GENE-171207-1	Melanosome biogenesis
ENSAOCG00000012295	*nsf1*	Beta-soluble NSF attachment protein-like	Melanosome biogenesis
ENSAOCG00000022013	*PMELb*	Melanocyte protein PMEL-like	Melanosome biogenesis
ENSAOCG00000017567	*PMELa*	PMELa	Melanosome biogenesis
ENSAOCG00000000169	*rabggta*	Rab geranylgeranyltransferase subunit alpha	Melanosome biogenesis
ENSAOCG00000018465	*snapin*	SNAP associated protein	Melanosome biogenesis
ENSAOCG00000006689	*th*	Tyrosine hydroxylase	Melanosome biogenesis
ENSAOCG00000001137	*txndc5*	Thioredoxin domain containing 5	Melanosome biogenesis
ENSAOCG00000019922	*vps33a*	VPS33A, CORVET/HOPS core subunit	Melanosome biogenesis
ENSAOCG00000008212	*vps39*	VPS39, HOPS complex subunit	Melanosome biogenesis
ENSAOCG00000014627	*atrn*	Attractin	Melanogenesis regulation
ENSAOCG00000016976	*clcn7*	chloride channel 7	Melanogenesis regulation
ENSAOCG00000006038	*drd2a*	dopamine receptor D2a	Melanogenesis regulation
ENSAOCG00000004549	*mc1r*	Melanocortin 1 receptor	Melanogenesis regulation
ENSAOCG00000022094	*mgrn1*	Mahogunin ring finger 1	Melanogenesis regulation
ENSAOCG00000014912	*nf1*	Neurofibromin 1	Melanogenesis regulation
ENSAOCG00000004657	*ostm1*	osteoclastogenesis associated transmembrane protein 1	Melanogenesis regulation
ENSAOCG00000003964	*POMCaa*	Pro-opiomelanocortin like	Melanogenesis regulation
ENSAOCG00000012931	*POMCab*	Pro-opiomelanocortin like	Melanogenesis regulation
ENSAOCG00000021637	*POMCb*	Pro-opiomelanocortin like	Melanogenesis regulation
ENSAOCG00000000919	*slc7a11*	solute carrier	Melanogenesis regulation
ENSAOCG00000012099	*zeb2a*	Zinc finger E-box-binding homeobox 2-like	Melanogenesis regulation
ENSAOCG00000009065	*zeb2b*	Zinc finger E-box-binding homeobox 2-like	Melanogenesis regulation
ENSAOCG00000009796	*adam17a*	Disintegrin and metalloproteinase domain-containing protein 17-like	Melanophores development
ENSAOCG00000022177	*adam17b*	Disintegrin and metalloproteinase domain-containing protein 17-like	Melanophores development
ENSAOCG00000015081	*dct (tyrp2)*	Dopachrome tautomerase	Melanophores development
ENSAOCG00000007456	*csf1ra*	Colony stimulating factor 1 receptor a	Melanophores development
ENSAOCG00000014365	*ednrb1a / rse**	Endotheline receptor beta a	Melanophores development
ENSAOCG00000018528	*ednrb2*	endothelin receptor type B-like	Melanophores development
ENSAOCG00000007874	*Erbb3b*	receptor tyrosine protein kinase ERbB3 like	Melanophores development
ENSAOCG00000021468	*gch2**	GTP cyclohydrolase 2	Melanophores development
ENSAOCG00000015421	*gfpt1*	Glutamine--fructose-6-phosphate aminotransferase	Melanophores development
ENSAOCG00000007998	*gja5a (CX40)*	gap junction protein, alpha 5a	Melanophores development

ENSAOCG00000021644	*hdac1*	Probable histone deacetylase 1-B	Melanophores development
ENSAOCG00000010518	*igsf11*	Immunoglobulin superfamily member 11	Melanophores development
ENSAOCG00000009335	*impdh1b*	Inosine-5,-monophosphate dehydrogenase 1a	Melanophores development
ENSAOCG00000014060	*kcnj13*	Potassium voltage-gated channel subfamily J member 13	Melanophores development
ENSAOCG00000005066	*kita*	KIT proto-oncogene receptor tyrosine kinase	Melanophores development
ENSAOCG00000017230	*kitlga*	KIT ligand	Melanophores development
ENSAOCG00000022699	*mitf*	Melanocyte inducing transcription factor	Melanophores development
ENSAOCG00000024679	*mitfa*	microphthalmia-associated transcription factor-like	Melanophores development
ENSAOCG00000012659	*mreg*	melanoregulin like	Melanophores development
ENSAOCG00000001912	*oca2**	oculocutaneous albinism 2	Melanophores development
ENSAOCG00000022048	*rnf41*	ring finger protein 41 also known as nrdp1	Melanophores development
ENSAOCG00000004478	*sf3b1*	Splicing factor 3b subunit 1	Melanophores development
ENSAOCG00000011884	*mtrex*	Mtr4 exosome RNA helicase	Melanophores development
ENSAOCG00000017491	*slc24a5*	Solute carrier family 24 member 5	Melanophores development
ENSAOCG00000012126	*slc45a2*	Solute carrier family 24 member 2	Melanophores development
ENSAOCG00000020276	*sox9**	SRY-box 9	Melanophores development
ENSAOCG00000003175	*sox10**	SRY-box 10	Melanophores development
ENSAOCG00000003676	*sox18*	Transcription factor Sox-18B-like	Melanophores development
ENSAOCG00000012209	*tfap2e*	Transcription factor AP-2 epsilon	Melanophores development
ENSAOCG00000024599	*trpm7*	Transient receptor potential cation channel subfamily M member 7	Melanophores development
ENSAOCG00000001583	*tyr*	Tyrosinase	Melanophores development
ENSAOCG00000015186	*tyrp1*	Tyrosinase related protein	Melanophores development
ENSAOCG00000020335	*vps11*	Vacuolar protein sorting 11	Melanophores development
ENSAOCG00000016327	*zic2a*	Zic family member 2	Melanophores development
ENSAOCG00000023827	*mlph*	melanophilin-like	Melanophores development
ENSAOCG00000006661	*foxd3*	Forkhead box D3	Melanophores development

259
260

Table S6: Significant differentially expressed genes between new recruits in *S. gigantea* and new recruits in *H. magnifica*. Positive logFC values correspond to an increased expression in recruits from *H. magnifica*, while negative logFC correspond to increased expression in recruits from *S. gigantea*.

Gene ID	log2FC	P.Value	adj.P.Val	Gene Name
ENSAPEG00000010017	-2,347318	1,7035E-06	0,01867009	dtx4a
ENSAPEG00000022337	4,08414	2,93817E-06	0,01867009	pde6ha
ENSAPEG00000021595	1,801743	2,76257E-06	0,01867009	cdk5rap2
ENSAPEG00000023092	-1,793328	4,42461E-06	0,02105089	tph1b
ENSAPEG00000011632	1,591216	8,55478E-06	0,02105089	cry1b
ENSAPEG00000024262	2,017805	1,23484E-05	0,02109894	opn1sw1
ENSAPEG00000017542	3,080685	1,32816E-05	0,02109894	pde6c
ENSAPEG00000023087	1,859143	8,62465E-06	0,02105089	Novel Gene
ENSAPEG00000004435	2,304421	1,09802E-05	0,02105089	Novel Gene
ENSAPEG00000020147	-1,559555	1,92966E-05	0,02610697	Novel Gene
ENSAPEG00000019637	2,026087	9,79215E-06	0,02105089	si:ch211-22d5.2
ENSAPEG00000012915	2,096826	2,07802E-05	0,02610697	opn1mw1
ENSAPEG00000021892	-1,997073	2,15436E-05	0,02610697	Novel Gene
ENSAPEG00000004911	-1,343448	2,19122E-05	0,02610697	Novel Gene
ENSAPEG00000019937	-1,119003	2,74051E-05	0,02902352	guca1a
ENSAPEG00000010570	-3,073506	6,02776E-06	0,02105089	si:ch211-133l11.10
ENSAPEG00000021151	3,687114	1,10428E-05	0,02105089	si:ch211-285j22.3
ENSAPEG00000013744	-1,650613	3,994E-05	0,03460802	phkg1a
ENSAPEG00000018502	2,273479	3,3486E-05	0,03359706	mpp4a
ENSAPEG00000003377	-2,983118	3,56368E-05	0,03396722	six7
ENSAPEG00000013880	-5,745882	5,09977E-05	0,03888679	Novel Gene
ENSAPEG00000008043	-1,273521	5,67158E-05	0,03964488	spsb3b
ENSAPEG00000024019	-2,528243	4,83352E-05	0,03839225	duox
ENSAPEG00000001204	-1,380617	5,90721E-05	0,03964488	dyrk4
ENSAPEG00000000862	-1,658533	4,77352E-05	0,03839225	Novel Gene
ENSAPEG00000010689	2,022108	6,09705E-05	0,03964488	Novel Gene
ENSAPEG00000000817	-1,630818	6,23903E-05	0,03964488	parp6b
ENSAPEG00000022071	-1,540916	6,9001E-05	0,04243117	trib3
ENSAPEG00000014635	-2,120314	6,18497E-05	0,03964488	aanat1
ENSAPEG00000024138	-2,654757	3,98474E-05	0,03460802	FIBCD1
ENSAPEG00000011641	-1,529507	8,38792E-05	0,04568542	mylpfb
ENSAPEG00000007251	-1,012826	8,91439E-05	0,04720417	nupr1b
ENSAPEG00000006869	3,432929	2,46978E-05	0,027695	aipl2
ENSAPEG00000012859	2,768406	8,37271E-05	0,04568542	slc1a8b
ENSAPEG00000022400	1,891581	8,20603E-05	0,04568542	rx2
ENSAPEG00000022686	-7,340735	7,89791E-05	0,04568542	Novel Gene

REFERENCES for SI

1. R. Patro, G. Duggal, M. I. Love, R. A. Irizarry, C. Kingsford, Salmon provides fast and bias-aware quantification of transcript expression. *Nat. Methods* **14**, 417–419 (2017).
2. C. Soneson, M. I. Love, M. D. Robinson, Differential analyses for RNA-seq: transcript-level estimates improve gene-level inferences. *F1000Research* **4**, 1521 (2016).
3. S. Anders, W. Huber, Differential expression analysis for sequence count data. *Genome Biol.* **11**, R106 (2010).
4. M. Martin, Cutadapt removes adapter sequences from high-throughput sequencing reads. *EMBnet.journal* **17**, 10 (2011).
5. N. Joshi, J. Fass, Sickle: A sliding-window, adaptive, quality-based trimming tool for FastQ files (Version 1.33) [Software]. *Available at https://github.com/najoshi/sickle.* (2011).
6. R. Lehmann, *et al.*, Finding nemo's genes: A chromosome-scale reference assembly of the genome of the orange clownfish Amphiprion percula. *Mol. Ecol. Resour.* **19**, 570–585 (2019).
7. D. Kim, B. Langmead, S. L. Salzberg, HISAT: a fast spliced aligner with low memory requirements. *Nat. Methods* **12**, 357–360 (2015).
8. S. Anders, P. T. Pyl, W. Huber, HTSeq--a Python framework to work with high-throughput sequencing data. *Bioinformatics* **31**, 166–169 (2015).
9. M. D. Robinson, D. J. McCarthy, G. K. Smyth, edgeR: a Bioconductor package for differential expression analysis of digital gene expression data. *Bioinformatics* **26**, 139–140 (2010).
10. C. W. Law, Y. Chen, W. Shi, G. K. Smyth, voom: precision weights unlock linear model analysis tools for RNA-seq read counts. *Genome Biol.* **15**, R29 (2014).
11. M. E. Ritchie, *et al.*, limma powers differential expression analyses for RNA-sequencing and microarray studies. *Nucleic Acids Res.* **43**, e47–e47 (2015).
12. N. Raventos, E. Macpherson, Planktonic larval duration and settlement marks on the otoliths of Mediterranean littoral fishes. *Mar. Biol.* **138**, 1115–1120 (2001).
13. K. P. Burnham, D. R. Anderson, *Model selection and multimodel inference* (Springer-Verlag New York, 2002).
14. M. R. E. Symonds, A. Moussalli, A brief guide to model selection, multimodel inference and model averaging in behavioural ecology using Akaike's information criterion. *Behav. Ecol. Sociobiol.* **65**, 13–21 (2011).
15. T. W. Arnold, Uninformative parameters and model selection using Akaike's Information Criterion. *J. Wildl. Manage.* **74**, 1175–1178 (2010).
16. H. Schielzeth, Simple means to improve the interpretability of regression coefficients.

303 *Methods Ecol. Evol.* **1**, 103–113 (2010).
304 17. G. Holzer, *et al.*, Fish larval recruitment to reefs is a thyroid hormone-mediated
305 metamorphosis sensitive to the pesticide chlorpyrifos. *Elife* **6** (2017).
306 18. M. Tagawa, T. Hirano, Changes in tissue and blood concentrations of thyroid
307 hormones in developing chum salmon. *Gen. Comp. Endocrinol.* **76**, 437–443 (1989).
308 19. I. E. Einarsdóttir, N. Silva, D. M. Power, H. Smáradóttir, B. T. Björnsson, Thyroid and
309 pituitary gland development from hatching through metamorphosis of a teleost flatfish,
310 the Atlantic halibut. *Anat. Embryol. (Berl).* **211**, 47–60 (2005).
311 20. Y. Kawakami, J. Nozaki, M. Seoka, H. Kumai, H. Ohta, Characterization of thyroid
312 hormones and thyroid hormone receptors during the early development of Pacific
313 bluefin tuna (Thunnus orientalis). *Gen. Comp. Endocrinol.* **155**, 597–606 (2008).
314 21. D. M. Parichy, M. R. Elizondo, M. G. Mills, T. N. Gordon, R. E. Engeszer, Normal table
315 of postembryonic zebrafish development: Staging by externally visible anatomy of the
316 living fish. *Dev. Dyn.* **238**, 2975–3015 (2009).
317 22. D. S. Eom, E. J. Bain, L. B. Patterson, M. E. Grout, D. M. Parichy, Long-distance
318 communication by specialized cellular projections during pigment pattern development
319 and evolution. *Elife* **4** (2015).
320 23. J. E. Spiewak, *et al.*, Evolution of Endothelin signaling and diversification of adult
321 pigment pattern in Danio fishes. *PLOS Genet.* **14**, e1007538 (2018).
322 24. K. Hoshijima, *et al.*, Highly efficient CRISPR-Cas9-based methods for generating
323 deletion mutations and F0 embryos that lack gene function in zebrafish. *Dev. Cell* **51**,
324 645-657.e4 (2019).
325 25. S. K. McMenamin, *et al.*, Thyroid hormone-dependent adult pigment cell lineage and
326 pattern in zebrafish. *Science (80-.).* **345**, 1358–1361 (2014).
327 26. T. Lorin, F. G. Brunet, V. Laudet, J.-N. Volff, Teleost fish-specific preferential retention
328 of pigmentation gene-containing families after whole genome duplications in
329 Vertebrates. *G3; Genes|Genomes|Genetics* **8**, 1795–1806 (2018).
330 27. I. Braasch, F. Brunet, J.-N. Volff, M. Schartl, Pigmentation pathway evolution after
331 whole-genome duplication in fish. *Genome Biol. Evol.* **1**, 479–493 (2009).
332